Engineering with Computers (2023) 39:2067–2087
https://doi.org/10.1007/s00366-021-01567-5

ORIGINAL ARTICLE

Damage identification of structural systems by modal strain energy and an optimization-based iterative regularization method

Mohammad Hassan Daneshvar[1] · **Mohsen Saffarian**[2] · **Hashem Jahangir**[3] · **Hassan Sarmadi**[1]

Received: 15 November 2020 / Accepted: 6 December 2021 / Published online: 31 January 2022

Abstract
Sensitivity-based methods using modal data are effective and reliable tools for damage localization and quantification. However, those may fail in obtaining reasonable and accurate results due to low damage detectability of sensitivity functions and the ill-posedness problem caused by noisy modal data. To address these major challenges, this article proposes a new method for locating and quantifying damage by developing a new sensitivity function of modal strain energy and solving an ill-posed inverse problem via an optimization-based iterative regularization method called Iteratively Reweighted Norm-Basis Pursuit Denoising (IRN-BPD). A stopping condition based on the residual of the solution and an improved generalized cross-validation function are proposed to terminate the iterative algorithm of IRN-BPD and determine an optimal regularization value. The major contributions of this article include getting an idea from the first-order necessary condition of the optimization problem for deriving a sensitivity formulation and proposing a new regularized solution. The great advantages of these methods are increasing damage detectability, determining an optimal regularization value, and obtaining an accurate solution. A simple mass–spring system and a full-scale bridge structure are considered to verify the accuracy and effectiveness of the proposed methods in numerical studies. Results demonstrate that the methods presented in this article succeed in locating and quantifying damage under incomplete noisy modal data.

Keywords Damage identification · Sensitivity analysis · Modal strain energy · Optimization · Regularization · Incomplete noisy modal data

1 Introduction

In civil engineering communities, vibration-based damage identification methods have received considerable attention due to the importance of the health and integrity of civil structures. From the civil engineers' perspective, the structural damage can occur with any deviation in geometry configurations, boundary conditions, and material deterioration leading to reductions in structural stiffness, undesirable stresses and displacements, inappropriate vibrations, failure, and even collapse. To prevent any catastrophic event and guarantee the safety and serviceability of civil structures, it is essential to perform Structural Health Monitoring (SHM) and damage diagnosis strategies for evaluating structural conditions as well as locating and quantifying damage using vibration data [1, 2].

Most of the vibration-based damage diagnosis methods are generally categorized into the three main levels including early damage detection (level 1), damage localization (level 2), and damage quantification (level 3). The first level is a global process aiming at perceiving whether the damage is available throughout the structure. Recently, this process is often implemented by data-based methods under machine learning aspects [3–6] due to some benefits [i.e., no finite-element (FE) modeling, system identification, model

✉ Hashem Jahangir
h.jahangir@birjand.ac.ir

Mohammad Hassan Daneshvar
hasan.daneshvar@mail.um.ac.ir

Mohsen Saffarian
saffarian@birjandut.ac.ir

Hassan Sarmadi
hassan.sarmadi@mail.um.ac.ir

[1] Department of Civil Engineering, Faculty of Engineering, Ferdowsi University of Mashhad, Mashhad, Iran

[2] Department of Computer and Industrial Engineering, Birjand University of Technology, Birjand, Iran

[3] Department of Civil Engineering, University of Birjand, Birjand, Iran

updating, data transformation, and incomplete data, etc.] against model-based techniques. The second and third levels are local, which are intended to identify the location of damage and then estimate or quantify the damage severity using both model-based [7, 8] and data-based [9, 10] methods. A large number of research efforts have been developed to detect structural damage using modal data including natural frequencies (eigenvalues), mode shapes (eigenvectors), and other modal-based characteristics. Because such dynamic features depend only on the inherent physical properties of a structure (i.e., mass, damping, and stiffness) regardless of excitation sources, the model-based damage identification is still a popular and effective approach [11].

Due to major advances in numerical modeling of structural systems through engineering software and importance of the local levels of damage diagnosis, it is preferable to locating and quantifying structural damage by the model updating or model-based strategy [7, 8, 12–14]. This is because data-based methods need a dense sensor network and accurate sensor placement for damage localization [15], and are not able to quantitatively estimate the severity of damage [16]. The fundamental principle of the model-based strategy is to adjust the inherent properties of a structure owing to differences between the dynamic characteristics (i.e., structural responses or modal data) of the FE and real models [17]. On this basis, it is assumed that the FE model reflects the normal or undamaged condition of the structure, while the real model is an unknown state, which can be either undamaged or damaged [8]. Under such concepts, the inherent structural properties and analytical modal parameters are simply obtained from the FE model, whereas the only experimental data are available in the real structure. Because the model updating strategy is an inverse problem and the relationship between the structural parameters and modal data is intrinsically nonlinear, sensitivity-based methods are developed to simplify the solution to this problem using the linearization of equations [18, 19].

The majority of model-based sensitivity functions have been proposed by taking the first-order derivative of the modal data with respect to structural parameters using the fundamental dynamic equations such as the generalized eigenvalue problem and orthogonality conditions [18]. It is well known that the measurement of the modal frequencies is simpler and more accurate than the mode shapes. However, the main drawback is that those are global vibration characteristics and may not give sufficient spatial information about damage [20]. This is due to the fact that the structural damage is an intrinsically local phenomenon. Hence, it is preferable to use the mode shapes in complicated and local problems such as damage localization and quantification. Although the application of the mode shape and its sensitivity to damage is reasonable, it is prominent to use a robust dynamic feature and a sensitivity function that should not only pertain to damage but also have high detectability [7]. One of them is the modal strain energy (MSE) that defines as a function of mode shapes and stiffness matrix [8, 11, 20]. In most cases, structural damage decreases the stiffness of the structure, while the mass often remains invariant. Therefore, one can utilize the MSE and its sensitivity formulations as efficient and reliable dynamic characteristics in early damage detection, localization, and quantification. Despite proposing various sensitivity functions of MSE [8, 21, 22], it is necessary to develop a new and efficient sensitivity function for increasing damage detectability and dealing with the limitations of some existing formulations, particularly the functions proposed by Entezami et al. [8] and Li et al. [22] that require additional unknown parameters (i.e., Lagrange multipliers) and fall in the parametric class of sensitivity formulations.

The other major challenge is related to the ill-posedness of the inverse problem of damage identification based on the model updating strategy [23]. This problem is often a linear mathematical system containing a coefficient matrix, which originates from a sensitivity function, the vector of residual between the undamaged and damaged dynamic characteristics, and unknown coefficients that should be determined [8]. Due to some reasons such as ill-conditioning and sparsity of the coefficient matrix and noise in measurements, the linear inverse problem is ill-posed. Regularization is an influential tool for addressing this challenge and solving the inverse problem stably [7, 17, 20, 23]. Generally, this process can be carried out by direct, iterative, and hybrid approaches.

Direct regularization methods are usually simple, easy-to-use without any particular complexity. These methods often aim at solving the ill-posed inverse problem in one-step procedures. Tikhonov regularization and truncated singular value decomposition are two well-known direct techniques [23]. Iterative methods are often divided into subspace iterative and optimization-based iterative approaches. The first method is based on the Krylov subspace theory and a bidiagonalization algorithm for solving an inverse problem [e.g., Least-Squares Minimal Residual (LSMR) utilized by Sarmadi et al. [24] for model updating]. In this regard, a subspace iterative technique attempts to repeat the solution of the inverse problem without any regularization parameter until a stopping condition to be satisfied. Typically, the number of iterations behaves as a regularization value [25]. The second method is an optimization problem that aims at minimizing a solution function consisting of the penalty and regularization terms in an iterative algorithm [26]. Finally, hybrid methods combine direct and iterative regularization algorithms for solving ill-posed inverse problems [7, 20].

Although the utilization of direct methods is usually simple without any complexity, it may not be sufficiently influential resulting from solving the ill-posed inverse problem once and their poor performances under noisy measurements

[8]. The major drawback of subspace iterative methods is that those may suffer from a semi-convergence behavior that affects the stability of the solution leading to their poor performances [27]. Despite accurate and reasonable results of hybrid methods, computational complexity stemming from the combination of two different regularized solution algorithms is the major limitation of these methods. In contrast, the optimization-based iterative methods have neither the drawbacks of the direct and subspace iterative techniques (i.e., unstable solutions and poor performances) nor the complexity of hybrid approaches.

The main objective of this article is to propose a new sensitivity-based method by deriving a new sensitivity function of MSE and solving an ill-posed inverse problem via an optimization-based iterative regularization method called Iteratively Reweighted Norm-Basis Pursuit Denoising (IRN-BPD). The major novelty of the proposed sensitivity function is to get an idea from the concept of the optimization problem and its first-order necessary condition. The main merits of this function are its high sensitivity to damage that increases damage detectability and its non-parametric property without any additional unknown parameter needed for deriving the sensitivity formulation. In this regard, a term concerning the variation in structural stiffness, which is taken into account as the main damage index, is added to the first-order derivatives of the eigenvalue (modal frequency) and eigenvector (mode shape), which are directly used in the proposed sensitivity formulation. Unlike Entezami et al. [8], who proposed an improved sensitivity function of MSE for the problem of damage detection by developing the sensitivity formulation of Li et al. [22], the proposed sensitivity function in this article is more efficient than the mentioned improved formulation. Although both the proposed and improved functions are suitable for damage identification, the main novelty of the proposed sensitivity function is its non-parametric characteristic. As described earlier, the sensitivity formulations in [8, 22] depend strongly on some unknown parameters (the Lagrange multipliers), which should be determined properly, so that inaccurate calculations of these parameters may cause inappropriate sensitivity functions and coefficient (sensitivity) matrices. In contrast, the sensitivity function of MSE proposed in this article not only enhances the detectability of damage but also provides a non-parametric class of sensitivity formulation without any dependency on unknown parameters. The great advantage of the proposed IRN-BPD method is to provide an effective and computationally efficient iterative algorithm for solving the ill-posed inverse problem of damage identification. Although IRN-BPD has originally been proposed by Rodriguez and Wohlberg [26], some deficiencies such as the lack of having a criterion for stopping condition and an approach to determining an optimal regularization parameter make it difficult to use in the damage diagnosis problems. In this article, therefore, the residual of the solution and an improved generalized cross-validation (GCV) function are presented to address the mentioned deficiencies of IRN-BPD and increase its applicability. The effectiveness and performance of the proposed methods are verified in numerical studies by a simple mass–spring system and the full-scale I-40 bridge. Furthermore, comparative studies are performed to evaluate the superiority of the proposed methods over some existing and well-known approaches. Results demonstrate that the methods presented here are successful in locating and quantifying damage under incomplete and noisy modal data and those are also superior to some classical techniques.

The remainder of this article is organized as follows. Section 2 describes the relation between the optimization problem and sensitivity analysis. In this section, one can realize how to obtain a sensitivity function via the fundamental principle of the optimization problem. Section 3 proposes the new sensitivity function of MSE. In Sect. 4, the inverse problem of damage identification is derived using the proposed sensitivity function and the discrepancy between the MSE of the undamaged and damaged conditions. Section 5 describes the proposed IRN-BPD method for solving the inverse problem of damage identification. In this section, the proposed stopping condition and the improved GCV function for determining an optimal regularization value are explained as well. In Sect. 6, the results of damage localization and quantification along with comparative studies are presented. Finally, Sect. 7 summarizes the main conclusions of this article.

2 Relation between optimization problem and sensitivity analysis

Optimization is a computational tool that intends to find the minimum or maximum value of an objective function [28]. This process can be implemented in constrained (either equality or inequality) and unconstrained problems. For the first class of optimization, the problem consists of the three basic ingredients: (i) the vector of variables $\mathbf{x} = [x_1 \ldots x_v]$, where v denotes the number of variables (ii) an objective or cost function $f(\mathbf{x})$, and (iii) equality and/or inequality constraints. In the second class of optimization, which requires no constraints, the problem includes two main ingredients: (i) the vector of variables $\mathbf{x}$, and (ii) the objective function $f(\mathbf{x})$ [28]. The fundamental principle of any optimization problem is to minimize the objective function $f(\mathbf{x})$ with or without constraints under the first-order and second-order necessary conditions [29]. In the first-order necessary condition, the main goal is to find a local minimum or maximum ($\hat{\mathrm{x}}$) of the objective function $f(\mathbf{x})$ by taking the first-order derivative or gradient of $f(\mathbf{x})$ at that local point as follows:

$$\nabla f(\hat{\mathbf{x}}) = \frac{\partial f}{\partial x_i} = 0, \tag{1}$$

where $i = 1,2,\ldots,v$. On the other hand, the second-order necessary condition of an optimization problem is intended to utilize the second-order derivative of the objective function at the local minimum and maximum. Because sensitivity analysis directly relates to the first-order derivative of any dynamical function with respect to structural parameters, one can realize that the first-order necessary condition of the optimization problem allows us to develop various sensitivity formulations by defining proper objective functions.

3 A new sensitivity function of modal strain energy

The proposed sensitivity function for damage identification is based on MSE. This is a modal-based dynamic function that is defined as energy stored in a structural system when the mode shapes are equivalent to nodal displacements. In addition, the MSE is directly related to the structural stiffness, which is known as the main damage index [8]. Given a structural system with n degrees-of-freedom (DOFs) and q elements, the MSE function in the ith mode is formulated as $MSE_i = ½(\boldsymbol{\varphi}_i^{\mathrm{T}}\mathbf{K}\boldsymbol{\varphi}_i)$, where $i = 1,2,\ldots,m$ refers to the number of measured modes; $\boldsymbol{\varphi}_i \in \Re^n$ and $\mathbf{K} \in \Re^{n\times n}$ are the vector of mode shape in the ith mode and the stiffness matrix, respectively. Assuming the jth stiffness parameter p_j of the structural stiffness $\mathbf{K}$, where $j = 1,2,\ldots,q$, the objective function required for the optimization problem can be defined as follows:

$$f(p_j) = MSE_i - \frac{1}{2}\boldsymbol{\varphi}_i^T\mathbf{K}\boldsymbol{\varphi}_i = 0. \tag{2}$$

Based on the first-order necessary condition of the optimization problem presented in Eq. (1), the sensitivity function of MSE in the ith mode with respect to the jth structural parameter p_j is written as follows:

$$\frac{\partial f(p_j)}{\partial p_j} = \frac{\partial MSE_i}{\partial p_j} - \frac{1}{2}\left(\left(\frac{\partial \boldsymbol{\varphi}_i}{\partial p_j}\right)^T\mathbf{K}\boldsymbol{\varphi}_i + \boldsymbol{\varphi}_i^T\frac{\partial \mathbf{K}}{\partial p_j}\boldsymbol{\varphi}_i + \boldsymbol{\varphi}_i^T\mathbf{K}\frac{\partial \boldsymbol{\varphi}_i}{\partial p_j}\right) = 0. \tag{3}$$

Since $\mathbf{K}\boldsymbol{\varphi}_i = \boldsymbol{\varphi}_i^{\mathrm{T}}\mathbf{K}$, Eq. (3) can be rewritten as

$$\frac{\partial f(p_j)}{\partial p_j} = \frac{\partial MSE_i}{\partial p_j} - \frac{1}{2}\left(\boldsymbol{\varphi}_i^T\frac{\partial \mathbf{K}}{\partial p_j}\boldsymbol{\varphi}_i + 2\boldsymbol{\varphi}_i^T\mathbf{K}\frac{\partial \boldsymbol{\varphi}_i}{\partial p_j}\right) = 0. \tag{4}$$

Unlike $\partial\mathbf{K}/\partial p_j$, the first-order derivative of the modal vector (the sensitivity of eigenvector) is unknown and should be determined. Although a large number of methods have been presented to formulate $\partial\boldsymbol{\varphi}_i/\partial p_j$, one of the well-known and effective ways is Nelson's technique [18]. The fundamental principle of this technique lies in taking the first-order derivative of the generalized eigenvalue problem $(\mathbf{K} - \lambda_i\mathbf{M})\boldsymbol{\varphi}_i = 0$, where λ_i and $\mathbf{M} \in \Re^{n\times n}$ are the ith eigenvalue (the square of natural frequency) and the mass matrix, respectively. Accordingly, the first-order derivative of this problem with respect to p_j is given by

$$(\mathbf{K} - \lambda_i\mathbf{M})\frac{\partial \boldsymbol{\varphi}_i}{\partial p_j} = \frac{\partial \lambda_i}{\partial p_j}\mathbf{M}\boldsymbol{\varphi}_i - \frac{\partial \mathbf{K}}{\partial p_j}\boldsymbol{\varphi}_i. \tag{5}$$

Since the mass matrix remains invariant during damage occurrence, one can neglect its derivative. As Eq. (5) appears, the sensitivity of mode shape depends on the derivative of the eigenvalue. Using the stiffness-orthogonality condition $\boldsymbol{\varphi}_i^{\mathrm{T}}\mathbf{K}\boldsymbol{\varphi}_i = \lambda_i$, the derivative of the eigenvalue with respect to the jth structural parameter p_j is expressed as

$$\frac{\partial \lambda_i}{\partial p_j} = \boldsymbol{\varphi}_i^T\frac{\partial \mathbf{K}}{\partial p_j}\boldsymbol{\varphi}_i + 2\boldsymbol{\varphi}_i^T\mathbf{K}\frac{\partial \boldsymbol{\varphi}_i}{\partial p_j}. \tag{6}$$

The first term of the right-hand side of Eq. (6) describes the variation in the structural stiffness that is known. This means that the unknown component in Eq. (6) is the derivative of mode shape that can be approximated by the rate of change in the global stiffness matrix as follows [30]:

$$\frac{\partial \boldsymbol{\varphi}_i}{\partial p_j} \cong \sum_{t=1}^{m}\frac{1}{\lambda_i - \lambda_t}\boldsymbol{\varphi}_t^T\frac{\partial \mathbf{K}}{\partial p_j}\boldsymbol{\varphi}_i\boldsymbol{\varphi}_t. \tag{7}$$

Therefore, the first-order derivative of the eigenvalue is developed as

$$\frac{\partial \lambda_i}{\partial p_j} = \boldsymbol{\varphi}_i^T\frac{\partial \mathbf{K}}{\partial p_j}\boldsymbol{\varphi}_i + 2\boldsymbol{\varphi}_i^T\mathbf{K}\sum_{t=1}^{m}\frac{1}{\lambda_i - \lambda_t}\boldsymbol{\varphi}_t^T\frac{\partial \mathbf{K}}{\partial p_j}\boldsymbol{\varphi}_i\boldsymbol{\varphi}_t. \tag{8}$$

By substituting Eqs. (8) into (5), one can obtain

$$(\mathbf{K} - \lambda_i\mathbf{M})\frac{\partial \boldsymbol{\varphi}_i}{\partial p_j} = \left(\boldsymbol{\varphi}_i^T\frac{\partial \mathbf{K}}{\partial p_j}\boldsymbol{\varphi}_i + 2\boldsymbol{\varphi}_i^T\mathbf{K}\sum_{t=1}^{m}\frac{1}{\lambda_i - \lambda_t}\boldsymbol{\varphi}_t^T\frac{\partial \mathbf{K}}{\partial p_j}\boldsymbol{\varphi}_i\boldsymbol{\varphi}_t\right)\mathbf{M}\boldsymbol{\varphi}_i - \frac{\partial \mathbf{K}}{\partial p_j}\boldsymbol{\varphi}_i. \tag{9}$$

Let $\boldsymbol{\Gamma}$ denotes the inverse of $\mathbf{K} - \lambda_i\mathbf{M}$. Rather than using the classical inverse problem, which may lead to an inaccurate inversion when the matrix $\mathbf{K} - \lambda_i\mathbf{M}$ is ill-conditioned, it is better to utilize the pseudo-inverse procedure based on the singular value decomposition (SVD) technique. For this purpose, one can define $(\mathbf{K} - \lambda_i\mathbf{M}) = \mathbf{A}\boldsymbol{\Sigma}\mathbf{B}^{\mathrm{T}}$, where $\boldsymbol{\Sigma}$ is a diagonal matrix. Thus, it can be concluded that $\boldsymbol{\Gamma} = \mathbf{B}\boldsymbol{\Sigma}^{+}\mathbf{A}^{\mathrm{T}}$, where "+" stands for the pseudo-inverse. On this basis, the enhanced form of the sensitivity of mode shape is expressed as

$$\frac{\partial \boldsymbol{\varphi}_i}{\partial p_j} = \boldsymbol{\Gamma}\left(\boldsymbol{\varphi}_i^T \frac{\partial \mathbf{K}}{\partial p_j}\boldsymbol{\varphi}_i + 2\boldsymbol{\varphi}_i^T \mathbf{K} \sum_{t=1}^{m} \frac{1}{\lambda_i - \lambda_t}\boldsymbol{\varphi}_t^T \frac{\partial \mathbf{K}}{\partial p_j}\boldsymbol{\varphi}_i\boldsymbol{\varphi}_t\right)\mathbf{M}\,\boldsymbol{\varphi}_i - \boldsymbol{\Gamma}\frac{\partial \mathbf{K}}{\partial p_j}\boldsymbol{\varphi}_i. \tag{10}$$

By inserting the above expression into Eq. (4), one can yield

$$\begin{aligned}\frac{\partial f(p_j)}{\partial p_j} = \frac{\partial MSE_i}{\partial p_j} &- \frac{1}{2}\boldsymbol{\varphi}_i^T \frac{\partial \mathbf{K}}{\partial p_j}\boldsymbol{\varphi}_i \\ &- \boldsymbol{\varphi}_i^T \mathbf{K}\boldsymbol{\Gamma}\left(\boldsymbol{\varphi}_i^T \frac{\partial \mathbf{K}}{\partial p_j}\boldsymbol{\varphi}_i\right)\mathbf{M}\boldsymbol{\varphi}_i + \boldsymbol{\varphi}_i^T \mathbf{K}\,\boldsymbol{\Gamma}\frac{\partial \mathbf{K}}{\partial p_j}\boldsymbol{\varphi}_i \\ &- \boldsymbol{\varphi}_i^T \mathbf{K}\,\boldsymbol{\Gamma}\left(2\boldsymbol{\varphi}_i^T \mathbf{K} \sum_{t=1}^{m} \frac{1}{\lambda_i - \lambda_t}\boldsymbol{\varphi}_t^T \frac{\partial \mathbf{K}}{\partial p_j}\boldsymbol{\varphi}_i\boldsymbol{\varphi}_t\right)\mathbf{M}\boldsymbol{\varphi}_i = 0.\end{aligned} \tag{11}$$

Since $\partial f(p_j)/\partial p_j = 0$, the proposed sensitivity function of MSE is presented here as follows:

$$\begin{aligned}\frac{\partial MSE_i}{\partial p_j} = \frac{1}{2}\boldsymbol{\varphi}_i^T \frac{\partial \mathbf{K}}{\partial p_j}\boldsymbol{\varphi}_i + \boldsymbol{\varphi}_i^T \mathbf{K}\boldsymbol{\Gamma}\left(\boldsymbol{\varphi}_i^T \frac{\partial \mathbf{K}}{\partial p_j}\boldsymbol{\varphi}_i\right)\mathbf{M}\boldsymbol{\varphi}_i - \boldsymbol{\varphi}_i^T \mathbf{K}\,\boldsymbol{\Gamma}\frac{\partial \mathbf{K}}{\partial p_j}\boldsymbol{\varphi}_i \\ + \boldsymbol{\varphi}_i^T \mathbf{K}\,\boldsymbol{\Gamma}\left(2\boldsymbol{\varphi}_i^T \mathbf{K} \sum_{t=1}^{m} \frac{1}{\lambda_i - \lambda_t}\boldsymbol{\varphi}_t^T \frac{\partial \mathbf{K}}{\partial p_j}\boldsymbol{\varphi}_i\boldsymbol{\varphi}_t\right)\mathbf{M}\boldsymbol{\varphi}_i.\end{aligned} \tag{12}$$

The great benefit of the proposed sensitivity function of MSE is that it only utilizes the inherent properties of the FE model (the mass and stiffness matrices), the modal data of the undamaged state, and the derivative of the stiffness matrix. It should be clarified that the derivative of mode shape presented in Eq. (7) can directly be inserted into Eq. (4) to address the limitation of that equation (the unavailability of $\partial \boldsymbol{\varphi}_i/\partial p_j$) and derive the classical sensitivity of MSE as follows:

$$\frac{\partial \overline{MSE_i}}{\partial p_j} = \frac{1}{2}\boldsymbol{\varphi}_i^T \frac{\partial \mathbf{K}}{\partial p_j}\boldsymbol{\varphi}_i + \boldsymbol{\varphi}_i^T \mathbf{K}\left(\sum_{t=1}^{m} \frac{1}{\lambda_i - \lambda_t}\boldsymbol{\varphi}_t^T \frac{\partial \mathbf{K}}{\partial p_j}\boldsymbol{\varphi}_i\boldsymbol{\varphi}_t\right). \tag{13}$$

Due to the importance of damage identification by a robust sensitivity function with high damage detectability, however, the proposed sensitivity of MSE in Eq. (12) not only presents a new formulation but also incorporates more components of the structural stiffness as the main damage index. Compared with the sensitivity functions of MSE proposed by Entezami et al. [8] and Li et al. [22], moreover, one can state that the proposed sensitivity function in this article is more efficient than those formulations due to no additional parameters (i.e., the Lagrange multipliers needed for their sensitivity functions) for establishing the proposed sensitivity formulation.

4 The sensitivity-based damage identification strategy

Once the formulation of the proposed sensitivity function has been completed, it is necessary to define an inverse problem of damage identification. One of the great advantages of the sensitivity-based methods is that the definition of the inverse problem of interest can be carried out by the formulation of the sensitivity function. It is well known that the perturbation of each structural parameter leads to changes in the structural stiffness and MSE. Using the first-order Taylor's series, such changes can be described as $\Delta\mathbf{K} = (\partial\mathbf{K}/\partial p_j)\Delta p_j$, and $\Delta MSE_i = (\partial MSE_i/\partial p_j)\Delta p_j$. On this basis, it is possible to expand the discrepancy of MSE by inserting the proposed sensitivity of MSE as follows:

$$\begin{aligned}\Delta MSE_i = \frac{1}{2}\boldsymbol{\varphi}_i^T \frac{\partial \mathbf{K}}{\partial p_j}\Delta p_j\boldsymbol{\varphi}_i + \boldsymbol{\varphi}_i^T \mathbf{K}\boldsymbol{\Gamma}\left(\boldsymbol{\varphi}_i^T \frac{\partial \mathbf{K}}{\partial p_j}\Delta p_j\boldsymbol{\varphi}_i\right)\mathbf{M}\boldsymbol{\varphi}_i \\ - \boldsymbol{\varphi}_i^T \mathbf{K}\boldsymbol{\Gamma}\frac{\partial \mathbf{K}}{\partial p_j}\Delta p_j\boldsymbol{\varphi}_i \\ + \boldsymbol{\varphi}_i^T \mathbf{K}\,\boldsymbol{\Gamma}\left(2\boldsymbol{\varphi}_i^T \mathbf{K} \sum_{t=1}^{m} \frac{1}{\lambda_i - \lambda_t}\boldsymbol{\varphi}_t^T \frac{\partial \mathbf{K}}{\partial p_j}\Delta p_j\boldsymbol{\varphi}_i\boldsymbol{\varphi}_t\right)\mathbf{M}\boldsymbol{\varphi}_i.\end{aligned} \tag{14}$$

Using the stiffness discrepancy matrix $\Delta\mathbf{K}$, one can express

$$\begin{aligned}\Delta MSE_i = \frac{1}{2}\boldsymbol{\varphi}_i^T \Delta\mathbf{K}\boldsymbol{\varphi}_i + \boldsymbol{\varphi}_i^T \mathbf{K}\boldsymbol{\Gamma}\left(\boldsymbol{\varphi}_i^T \Delta\mathbf{K}\boldsymbol{\varphi}_i\right)\mathbf{M}\boldsymbol{\varphi}_i - \boldsymbol{\varphi}_i^T \mathbf{K}\,\boldsymbol{\Gamma}\,\Delta\mathbf{K}\boldsymbol{\varphi}_i \\ + \boldsymbol{\varphi}_i^T \mathbf{K}\,\boldsymbol{\Gamma}\left(2\boldsymbol{\varphi}_i^T \mathbf{K} \sum_{t=1}^{m} \frac{1}{\lambda_i - \lambda_t}\boldsymbol{\varphi}_t^T \Delta\mathbf{K}\boldsymbol{\varphi}_i\boldsymbol{\varphi}_t\right)\mathbf{M}\boldsymbol{\varphi}_i.\end{aligned} \tag{15}$$

On the other hand, the stiffness discrepancy matrix can be obtained by the difference between the local stiffness matrices of the damaged and undamaged structures. Since the stiffness matrix of the damaged state is unknown, one can write $\Delta\mathbf{K} = \sum_{j=1}^{q} \alpha_j \mathbf{k}_j$, where $\alpha_j < 0$ and $\mathbf{k}_j \in \Re^{n\times n}$ represent the stiffness reduction factor and local stiffness matrix of the jth element, respectively. Thus, Eq. (15) can be rewritten as

$$\begin{aligned}\Delta MSE_i = \frac{1}{2}\boldsymbol{\varphi}_i^T \left(\sum_{j=1}^{q} \alpha_j \mathbf{k}_j\right)\boldsymbol{\varphi}_i \\ + \boldsymbol{\varphi}_i^T \mathbf{K}\boldsymbol{\Gamma}\left(\boldsymbol{\varphi}_i^T \left(\sum_{j=1}^{q} \alpha_j \mathbf{k}_j\right)\boldsymbol{\varphi}_i\right)\mathbf{M}\boldsymbol{\varphi}_i \\ - \boldsymbol{\varphi}_i^T \mathbf{K}\,\boldsymbol{\Gamma}\left(\sum_{j=1}^{q} \alpha_j \mathbf{k}_j\right)\boldsymbol{\varphi}_i \\ + \boldsymbol{\varphi}_i^T \mathbf{K}\,\boldsymbol{\Gamma}\left(2\boldsymbol{\varphi}_i^T \mathbf{K} \sum_{t=1}^{m} \frac{1}{\lambda_i - \lambda_t}\boldsymbol{\varphi}_t^T \left(\sum_{j=1}^{q} \alpha_j \mathbf{k}_j\right)\boldsymbol{\varphi}_i\boldsymbol{\varphi}_t\right)\mathbf{M}\boldsymbol{\varphi}_i.\end{aligned} \tag{16}$$

Since α is a scalar value, the above equation can be modified as

$$\Delta MSE_i = \sum_{j=1}^{q} \alpha_j \left(\frac{1}{2} \boldsymbol{\varphi}_i^T \mathbf{k}_j \boldsymbol{\varphi}_i + \boldsymbol{\varphi}_i^T \mathbf{K} \boldsymbol{\Gamma} \left(\left(\boldsymbol{\varphi}_i^T \mathbf{k}_j \boldsymbol{\varphi}_i + 2 \boldsymbol{\varphi}_i^T \mathbf{K} \sum_{t=1}^{m} \frac{\boldsymbol{\varphi}_t^T \mathbf{k}_j \boldsymbol{\varphi}_i \boldsymbol{\varphi}_t}{\lambda_i - \lambda_t} \right) \mathbf{M} \boldsymbol{\varphi}_i - \mathbf{k}_j \boldsymbol{\varphi}_i \right) \right). \tag{17}$$

Additionally, the discrepancy of MSE is formulated in the following form:

$$\Delta MSE_i = \frac{1}{2} \sum_{j=1}^{q} \left(\hat{\boldsymbol{\varphi}}_i^T \hat{\mathbf{k}}_j \hat{\boldsymbol{\varphi}}_i - \boldsymbol{\varphi}_i^T \mathbf{k}_j \boldsymbol{\varphi}_i \right), \tag{18}$$

where $\hat{\boldsymbol{\varphi}}_i \in \Re^n$ and $\hat{\mathbf{k}}_j \in \Re^{n \times n}$ denote the ith mode shape and the local stiffness matrix of the jth element regarding the damaged state, respectively. An important note is that the mode shapes of the undamaged and damaged states should originate from the same physical condition [19]. This means that the modal vectors of these states should be mass normalized. Since the global mass matrix of the FE model regarding the undamaged condition is available, the mode shapes of this condition are always mass normalized, while this situation is not valid for the modal vector concerning the damaged state related to the real structure. Therefore, it needs to normalize the mode shapes of both the undamaged and damaged conditions by the modal scale factor [8]. The other important issue is the incompleteness of the modal displacements of the damaged state, which are usually available at a few DOFs. To address this limitation, one can exploit the System-Equivalent-Reduction-Expansion-Process (SEREP) technique [8] to expand the normalized mode shapes of the damaged structure. On the other hand, since the local stiffness matrix of the damaged state in Eq. (18) is mainly unknown, one can express it as $\hat{\mathbf{k}}_j = (1 - \alpha_j)\mathbf{k}_j$. Hence, the discrepancy of MSE is rewritten as follows:

$$\Delta MSE_i = \frac{1}{2} \left(\sum_{j=1}^{q} \hat{\boldsymbol{\varphi}}_i^T \mathbf{k}_j \hat{\boldsymbol{\varphi}}_i - \sum_{j=1}^{q} \boldsymbol{\varphi}_i^T \mathbf{k}_j \boldsymbol{\varphi}_i - \sum_{j=1}^{q} \alpha_j \hat{\boldsymbol{\varphi}}_i^T \mathbf{k}_j \hat{\boldsymbol{\varphi}}_i \right). \tag{19}$$

By substituting Eqs. (19) into (17) and arranging the terms related to the stiffness reduction factor, the inverse problem of damage identification is formulated as $\mathbf{Sa} = \mathbf{r}$. In this problem, $\mathbf{S} \in \Re^{m \times q}$, $\mathbf{a} = [\alpha_1 \ldots \alpha_q]^{\mathrm{T}} \in \Re^q$, and $\mathbf{r} = [r_1 \ldots r_m]^{\mathrm{T}} \in \Re^m$ are the sensitivity (coefficient) matrix of MSE obtained from the proposed sensitivity function, the vector of q stiffness reduction factors, and the residual vector of the MSE discrepancy values, respectively. Accordingly, the ith row and jth column of the sensitivity matrix $\mathbf{S}$ and the ith element of the residual vector $\mathbf{r}$ are given by

$$S_{ij} = \boldsymbol{\varphi}_i^T \mathbf{k}_j \boldsymbol{\varphi}_i + \hat{\boldsymbol{\varphi}}_i^T \mathbf{k}_j \hat{\boldsymbol{\varphi}}_i + 2 \boldsymbol{\varphi}_i^T \mathbf{K} \boldsymbol{\Gamma} \left(\left(\boldsymbol{\varphi}_i^T \mathbf{k}_j \boldsymbol{\varphi}_i + 2 \boldsymbol{\varphi}_i^T \mathbf{K} \sum_{t=1}^{m} \frac{\boldsymbol{\varphi}_t^T \mathbf{k}_j \boldsymbol{\varphi}_i \boldsymbol{\varphi}_t}{\lambda_i - \lambda_t} \right) \mathbf{M} \boldsymbol{\varphi}_i - \mathbf{k}_j \boldsymbol{\varphi}_i \right), \tag{20}$$

$$r_i = \sum_{j=1}^{q} \hat{\boldsymbol{\varphi}}_i^T \mathbf{k}_j \hat{\boldsymbol{\varphi}}_i - \sum_{j=1}^{q} \boldsymbol{\varphi}_i^T \mathbf{k}_j \boldsymbol{\varphi}_i. \tag{21}$$

Therefore, the main objective is to solve the inverse problem $\mathbf{Sa} = \mathbf{r}$ and determine the vector $\mathbf{a}$. In this regard, it is expected that the undamaged areas of the structure have the stiffness reduction factors equal or close to zero. Furthermore, the damage locations are then identified by finding elements with the largest stiffness reduction factors.

5 An optimization-based iterative regularization method

5.1 Regularization of ill-posed problems

The main objective of any regularization technique is to find an approximate solution of an inverse problem in the form of $\mathbf{Sa}_{\text{exact}} = \mathbf{r}_{\text{exact}}$, where $\mathbf{a}_{\text{exact}}$ and $\mathbf{r}_{\text{exact}}$ refer to the exact solution and the noise-free data, respectively. An important note is that both the vectors $\mathbf{a}_{\text{exact}}$ and $\mathbf{r}_{\text{exact}}$ are rare in practice due to the presence of noise. In other words, noise in data causes that the exact solution to $\mathbf{Sa}_{\text{exact}} = \mathbf{r}_{\text{exact}}$ is unavailable owing to unavailability of $\mathbf{r}_{\text{exact}}$. Therefore, one attempts to solve the ill-posed problem $\mathbf{Sa} = \mathbf{r}$, where each of the components of the vector $\mathbf{r}$ can be expressed as $r = r_{\text{exact}} + \varepsilon$; $\mathbf{a}$ is the approximate solution of $\mathbf{a}_{\text{exact}}$ and ε is the noise, by a regularization method under the principle of perturbation theory [31]. Based on this theory, the solution of $\mathbf{Sa} = \mathbf{r}$ is very sensitive to any perturbation (noise) in data (i.e., the vector $\mathbf{r}$) that makes the problem of interest ill-posed leading to an unreliable and unstable solution. Under inevitable circumstances of the presence of noise in data, regularization methods are used to filter the perturbation influences caused by noise, such that the solution is less dominated by the noise [31].

More precisely, these methods are called regularization methods, because they enforce regularity on the solution. By enforcing this regularity (smoothness), one can suppress some of the noise components leading to a more stable approximate solution. In this regard, the regularization value is added to control the stability of the solution and approach to the exact solution. On this basis, it is well known that

one can compute an approximation to $\mathbf{a}_{\text{exact}}$ by means of an effective regularization method and a proper regularization parameter that leads to much less sensitivity to the perturbations in data [31]. Therefore, regularization methods should be considered to reduce the influence noise and solve ill-posed problems. In this case, the regularization parameter plays a crucial role in providing both accuracy and stability of solution.

Tikhonov regularization is one of the well-known and classical regularized solution techniques that utilizes a regularization value for controlling the stability of an ill-posed inverse problem. Generally, this technique is based on minimizing a least-square problem comprising the penalty term $\|\mathbf{Sa}-\mathbf{r}\|_2$ and the regularization term $\gamma\|\mathbf{a}\|_2$, where γ denotes the regularization parameter. The penalty term measures the goodness-of-fit, which means how well the solution $\mathbf{a}$ predicts the given (noisy) data $\mathbf{r}$. Obviously, if this term is large, then, the vector $\mathbf{a}$ cannot be considered as a good solution in the sense that the problem of interest has not been solved properly. The regularization term adds a weight through the regularization value γ to the norm of the solution, so that it controls the regularity of the solution and plays a critical role in reducing the effect of noise. In this case, the balance between the terms of accuracy (i.e., the small value of the penalty term) and stability (i.e., the regularity of the solution) is controlled by the regularization parameter [31].

5.2 IRN-BPD

The proposed IRN-BPD method is an optimization tool for solving the ill-posed linear problems such as $\mathbf{Sa}=\mathbf{r}$, where $\mathbf{S}$ is a rectangular matrix ($m<q$), and the vector $\mathbf{r}$ includes unwanted and unknown noise levels in measurements (i.e., the mode shapes of the damaged structure). This technique is based on minimizing an l_2 penalty (fidelity) term subjected to an l_1 regularization term (sparsity constraint) in the following form [26]:

$$\min_{\mathbf{a}} \frac{1}{2}\|\mathbf{Sa}-\mathbf{r}\|_2^2+\gamma\|\mathbf{a}\|_1, \tag{22}$$

where $\frac{1}{2}\|\mathbf{Sa}-\mathbf{r}\|_2^2$ and $\|\mathbf{a}\|_1$ refer to the penalty and regularization terms, respectively. On this basis, the proposed IRN-BPD method is similar to the well-known Tikhonov regularization technique. The main objective of IRN-BPD is to map $\mathbf{Sa}=\mathbf{r}$ to a quadratic algorithm and solve it iteratively [26]. At the iteration k, this algorithm is based on a quadratic function as follows:

$$Q_k=\frac{1}{2}\left\|\mathbf{W}_k^{1/2}(\mathbf{Sa}-\mathbf{r})\right\|_2^2+\frac{\gamma_k}{2}\left\|\overline{\mathbf{W}}_k^{1/2}\mathbf{a}\right\|_2^2. \tag{23}$$

In this equation, $\mathbf{W}_k=\text{diag}(\mathbf{Sa}_k-\mathbf{r})$ and $\overline{\mathbf{W}}_k=\text{diag}(\tau(x))$ are the weighting diagonal matrices of the penalty and regularization terms at the kth iteration. For the variable x, moreover, $\tau(x)$ is a function equal to 1 for $|x|>\varepsilon$ and 0 for $|x|\le\varepsilon$, where ε is a small positive scalar. To minimize Eq. (23), it is necessary to move the weighting diagonal matrix $\overline{\mathbf{W}}_k$ from the regularization term into the penalty term. By setting $\mathbf{a}_k=\overline{\mathbf{W}}_k^{1/2}\mathbf{v}_k$, Eq. (23) can be rewritten as

$$Q_k=\frac{1}{2}\left\|\mathbf{W}_k^{1/2}\mathbf{S}\,\overline{\mathbf{W}}_k^{1/2}\mathbf{v}_k-\mathbf{W}_k^{1/2}\mathbf{r}\right\|_2^2+\frac{\gamma_k}{2}\|\mathbf{v}_k\|_2^2, \tag{24}$$

where $\mathbf{v}_k=\overline{\mathbf{W}}_k^{1/2}\mathbf{S}^{\mathrm{T}}\mathbf{u}_k$. In this expression, the vector $\mathbf{u}_k$ is given by

$$\mathbf{u}_k=\left(\mathbf{S}\,\overline{\mathbf{W}}_k^{-1}\mathbf{S}^T+\gamma_k\mathbf{W}_k^{-1}\right)^{-1}\mathbf{r}. \tag{25}$$

At the iteration $k=0,1,2,\ldots$, the vector $\mathbf{u}_k$ is initially substituted into the expression of $\mathbf{v}_k$. Subsequently, this vector is replaced to the expression of $\mathbf{a}_k=\overline{\mathbf{W}}_k^{1/2}\mathbf{v}_k$ to obtain the final solution of the linear ill-posed problem in the following form:

$$\mathbf{a}_k=\tilde{\mathbf{W}}_k^{-1}\mathbf{S}^T\left(\mathbf{S}\,\overline{\mathbf{W}}_k^{-1}\mathbf{S}^T+\gamma_k\mathbf{W}_k^{-1}\right)^{-1}\mathbf{r}, \tag{26}$$

where $\tilde{\mathbf{W}}_k=\text{diag}(\tau(\mathbf{a}_k))$ and $\tau(.)$ has been described earlier. The criterion for stopping the iterative algorithm is to compare the l_2-norm of the residual of solution $\|\boldsymbol{\delta}_k\|_2=\|\mathbf{Sa}_k-\mathbf{r}\|_2$ with an insubstantial scalar value e. On this basis, the iterative algorithm terminates when $\|\boldsymbol{\delta}_k\|_2<e$. The other important issue is related to the initialization of the IRN-BPD method, which requires the initial solution vector $\mathbf{a}_0$ when $k=0$. To address this problem, the initial solution vector can be defined as follows:

$$\mathbf{a}_0=\mathbf{S}^T\left(\mathbf{S}\,\mathbf{S}^T+\gamma\,\mathbf{I}\right)^{-1}\mathbf{r}, \tag{27}$$

where $\mathbf{I}\in\Re^{m\times m}$ is the identity matrix. It should be clarified that Eq. (27) is equivalent to the regularized solution by the Tikhonov regularization technique [31]. On the other hand, although the proposed method follows the same strategy as the classical Tikhonov regularization by minimizing the penalty and regularization terms, there are some advantages that make it superior to that classical technique. First, the Tikhonov regularization presents a direct regularized solution, which means that it solves the ill-posed inverse problem one time. Despite computational efficiency of this procedure, the comparative studies in this study (see Sects. 6.1 and 6.2) demonstrate that the proposed method provides more reliable results than the Tikhonov regularization. Second, the regularization parameters used in both the IRN-BPD and Tikhonov regularization (and other regularization techniques) add weights to the solutions of any ill-posed inverse problem. For this reason, they are able to better solve such problem and provide more accurate results in comparison

with non-regularized solution techniques. Nonetheless, the comparison between Eqs. (26) and (27) concerning the regularized solutions by IRN-BPD and Tikhonov regularization, respectively, reveals that the proposed method adds more weights on the solution of the ill-posed problem, not only on the regularization term but also on the penalty term. Therefore, it can be observed in the results of the comparative studies that the proposed IRN-BPD method outperforms the classical Tikhonov regularization with smaller computational errors due to its iterative nature and considering more weights.

5.3 Determination of an optimal regularization parameter

The regularization parameter is a crucial component of each regularized solution method [32]. An optimal regularization value enables the method of interest to solve the ill-posed inverse problem appropriately and obtain a stable solution [25]. When the regularized solution technique is non-iterative, it is possible to determine the regularization parameter one time. However, this approach may not be sufficiently suitable for iterative regularization methods, for which the solution of the inverse problem varies at each iteration. For this reason, this article proposes an algorithm based on an improved GCV function with the aid of IRN-BPD for choosing the optimal regularization parameter γ_k. Having considered the sensitivity matrix $\mathbf{S}$ and the vector $\mathbf{r}$, the general form of the GCV function is given by [25]

$$\mathrm{GCV}(\gamma) = \frac{\left\| \left(\mathbf{I} - \mathbf{S}\mathbf{S}_{\gamma}^{\#} \right) \mathbf{r} \right\|_2^2}{\left(\mathrm{trace}\left(\mathbf{I} - \mathbf{S}\mathbf{S}_{\gamma}^{\#} \right) \right)^2}, \tag{28}$$

where $\mathbf{S}^{\#}$ stands for the matrix that maps the vector $\mathbf{r}$ onto the regularized solution $\mathbf{a}$. The utilization of this function for obtaining the regularization parameter has two main limitations. First, the determination of the matrix $\mathbf{S}^{\#}$ depends on the type of regularization technique. Second, this function is often useful for non-iterative regularized solution methods. The first limitation can be dealt with using the residual of the solution $\boldsymbol{\delta}_k$ rather than $(\mathbf{I}-\mathbf{S}\mathbf{S}^{\#})\mathbf{r}$ in the numerator of Eq. (28) and the SVD of the sensitivity matrix for the denominator of this equation, that is

$$\mathrm{trace}\left(\mathbf{I} - \mathbf{S}\mathbf{S}_{\gamma}^{\#} \right) = m - \sum_{j=1}^{q} \frac{\sigma_j^2}{\sigma_j^2 + \gamma_k^2}, \tag{29}$$

where σ_j is the jth singular value of the sensitivity matrix after using the SVD. Therefore, the improved GCV function for the IRN-BPD method is expressed as follows:

$$\mathrm{GCV}\left(\gamma_k\right) = \frac{\left\| \boldsymbol{\delta}_k \right\|_2^2}{\left(m - \sum_{j=1}^{q} \frac{\sigma_j^2}{\sigma_j^2 + \gamma_k^2} \right)^2}. \tag{30}$$

The determination of an optimal regularization parameter is based on minimizing the improved GCV function. Since this function depends on the iteration number k, the procedures of stopping condition and regularization value determination are implemented in a simultaneous manner. This means that an initial regularization parameter is first computed by minimizing the GCV function of the non-iterative approach. Next, this regularization parameter is incorporated into the algorithm of the IRN-BPD method to obtain the solution residual at the first iteration. In most cases, since the l_2-norm of this residual is not usually smaller than the predefined quantity e, the inverse problem is solved by determining a new regularization parameter by minimizing Eq. (30) at a new iteration. This procedure continues until the iterative algorithm of IRN-BPD terminates on the basis of the stopping condition $\|\boldsymbol{\delta}_k\|_2 < e$. In this regard, the last regularization value at the iteration k is chosen as the optimal value.

6 Numerical models

6.1 The mass–spring system

To demonstrate the correctness and efficiency of the proposed methods in damage identification, a simple mass–spring system with six elements and DOFs ($q=n=6$) is considered, as shown in Fig. 1. Assume that the mass and stiffness of each element correspond to 1000 kg and 2000 KN/m, respectively. Given such physical properties, the global mass and stiffness matrices of the numerical model are simply obtained by the basic formulations related to discrete dynamical systems. The generalized eigenvalue

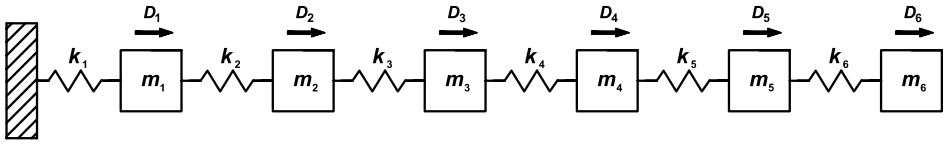

Fig. 1 The mass–spring system (m: Mass, k: Stiffness, and D: DOF)

problem is then applied to extract the modal frequencies and mode shapes.

The stiffness values of some elements are reduced to define two damage cases. For the first one, the stiffness quantities of the first and second elements decrease by 10% and 25%. In the second case, the stiffness values of the first–sixth elements reduce by 10%, 20%, 30%, 35%, 40%, and 50%, respectively. Using the generalized eigenvalue problem, the modal parameters of the damaged conditions are obtained, as well. To simulate a realistic condition, the first three modal frequencies ($m=3$) along with the modal displacements at the first, second, and fourth DOFs are selected to consider the incompleteness conditions of modal data. Another simulation is to incorporate noise in the selected modal displacements of the damaged structure. Since the modal frequencies of the damaged state are not available in the sensitivity matrix **S** and the residual vector **r**, different noise levels are only applied to the selected mode shapes. For the numerical problems, the noisy modal vector is simply simulated as follows:

$$\overline{\boldsymbol{\varphi}}_i = \overline{\boldsymbol{\varphi}}_i^* + \eta\, \mathbf{w}, \tag{31}$$

where η denotes the noise level; **w** is a randomly normal distribution vector with the same dimension as the mode shape. Based on the descriptions in Sect. 5.1, each value of ηw is equivalent to ε. Furthermore, $\overline{\boldsymbol{\varphi}}_{\mathrm{i}}$ and $\overline{\boldsymbol{\varphi}}_{\mathrm{i}}^*$ are the incomplete mode shapes of the damaged state in the ith mode associated with the noisy and noise-free conditions, respectively. For the mass–spring system, the noise levels equal to 1%, 3%, 5%, and 10% are considered to apply to the incomplete mode shapes of the damaged structure. Finally, each of the incomplete modal vectors is normalized by the modal scale factor and then expanded through the SEREP technique to obtain the vector $\hat{\boldsymbol{\varphi}}_i$.

Using all requirements for establishing the proposed sensitivity function of MSE and assuming that the stiffness matrices of the damaged conditions are available, Fig. 2 illustrates the damage detectability of the proposed sensitivity function in both damage cases in the 10% noise level. From Fig. 2a, it can be realized that the amounts of sensitivity matrix at the first and second elements are more than the other ones, which are roughly identical to zero. Furthermore, it can be observed in Fig. 2b that the minimum and maximum changes in the values of **S** have occurred at the first and sixth elements, which have the smallest and largest stiffness reduction factors. As another important observation, one can discern that the sensitivity quantity increases from the elements 1–6. All the obtained results in Fig. 2 prove that the proposed sensitivity function of MSE is sensitive to damage.

By constructing the sensitivity matrix **S** and the residual vector **r**, the inverse problem of damage identification is solved by the proposed IRN-BPD method to compute the vector of the estimated stiffness reduction factors **a**. Accordingly, Table 1 lists the number of iterations needed for the solution of the inverse problem $\mathbf{Sa}=\mathbf{r}$. Figure 3 illustrates the convergence rates of the solution of the inverse problem using the l_2-norm of $\boldsymbol{\delta}_k$ in Cases 1 and 2 for all noise levels. The stopping criterion for terminating the iterative algorithm is set as $e=1\mathrm{e}{-7}$. Furthermore, Fig. 4 shows the optimal regularization values in Case 1 for the 3% and 10% noise levels, respectively. From Fig. 4, one can observe that the regularization values at the last iterations ($k=34$ in Fig. 4a and $k=60$ in Fig. 4b) are chosen as the optimal quantities. The results of damage localization and quantification by the proposed methods (i.e., the proposed sensitivity function and IRN-BPD) in the first and second cases are shown in Fig. 5.

Table 1 The iteration numbers for solving the inverse problem of damage identification by IRN-BPD

Noise levels (%)	Case no.	
	1	2
0	22	21
1	34	33
3	34	32
5	46	51
10	60	63

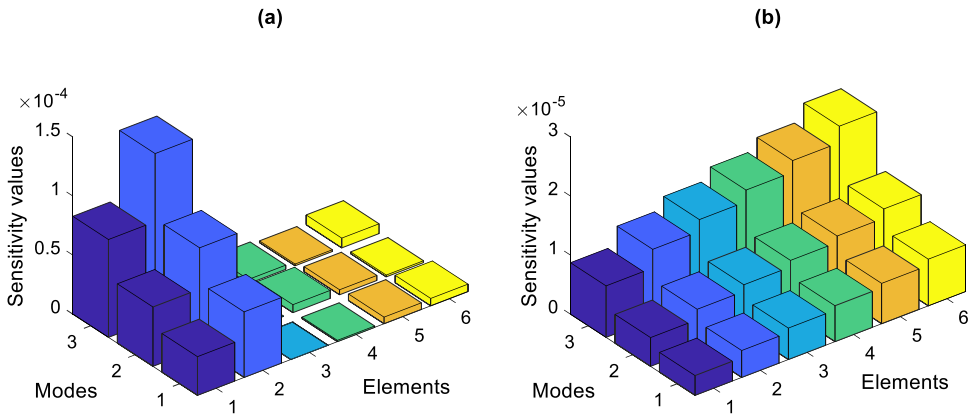

Fig. 2 Damage detectability of the proposed sensitivity function of MSE: **a** Case 1 and **b** Case 2

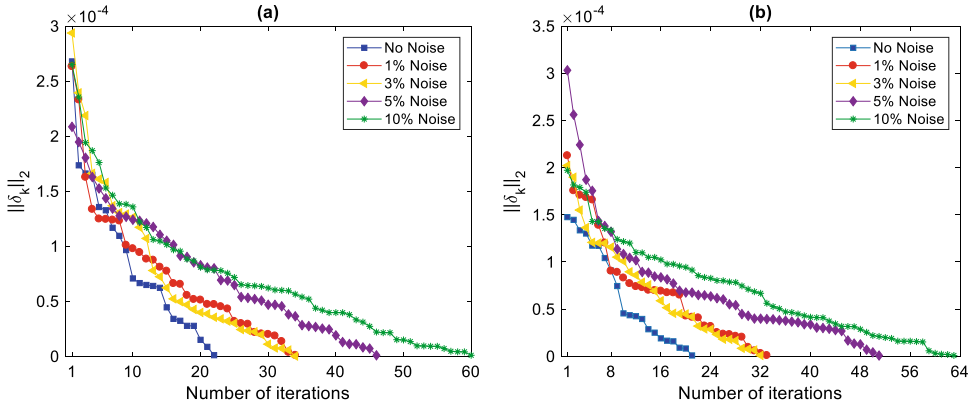

Fig. 3 Convergence rates of the solution of the inverse problem using the l_2-norm of $\boldsymbol{\delta}_k$: **a** Case 1 and **b** Case 2

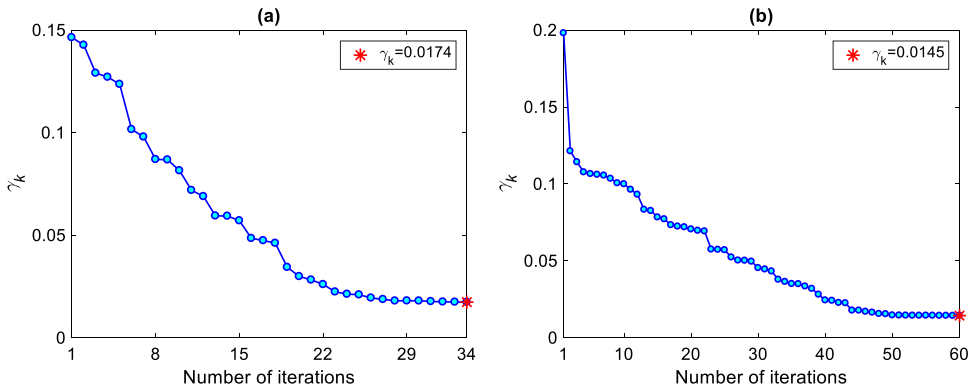

Fig. 4 Determination of the optimal regularization parameters via the improved GCV function in Case 1: **a** 3% noise level; **b** 10% noise level

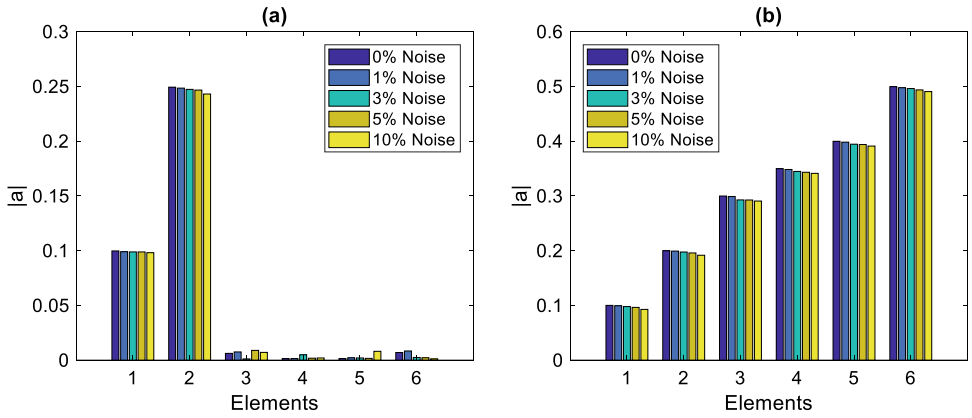

Fig. 5 Damage localization and quantification in the mass–spring system: **a** Case 1 and **b** Case 2

In Fig. 5a, it is clear that the first and second elements are the damage locations and their estimated stiffness reduction factors in the noise-free and noisy conditions are in good agreement with the actual reduction values (i.e., 10% and 25%), while the other elements approximately have zero reduction factors. As Fig. 5b illustrates, all elements of the mass–spring system are identified as the damage locations and one can discern that the estimated values in |**a**| are similar to their actual quantities implying the accurate quantification of the damage severities in Case 2. Therefore, these results confirm that the proposed methods in this article are able to localize the damaged areas of the system and accurately quantify the damage severities.

Despite reasonable results of damage localization and quantification, it would be very appropriate to compare the proposed methods with their counterparts. For this purpose, the relative error between the actual and estimated values of the stiffness reduction factor is applied to define a criterion for the comparison. First, the proposed sensitivity function of MSE is compared with the classical sensitivity formulation, as presented in Eq. (13), the function proposed by Yan and Ren [21]. Since the sensitivity functions proposed by

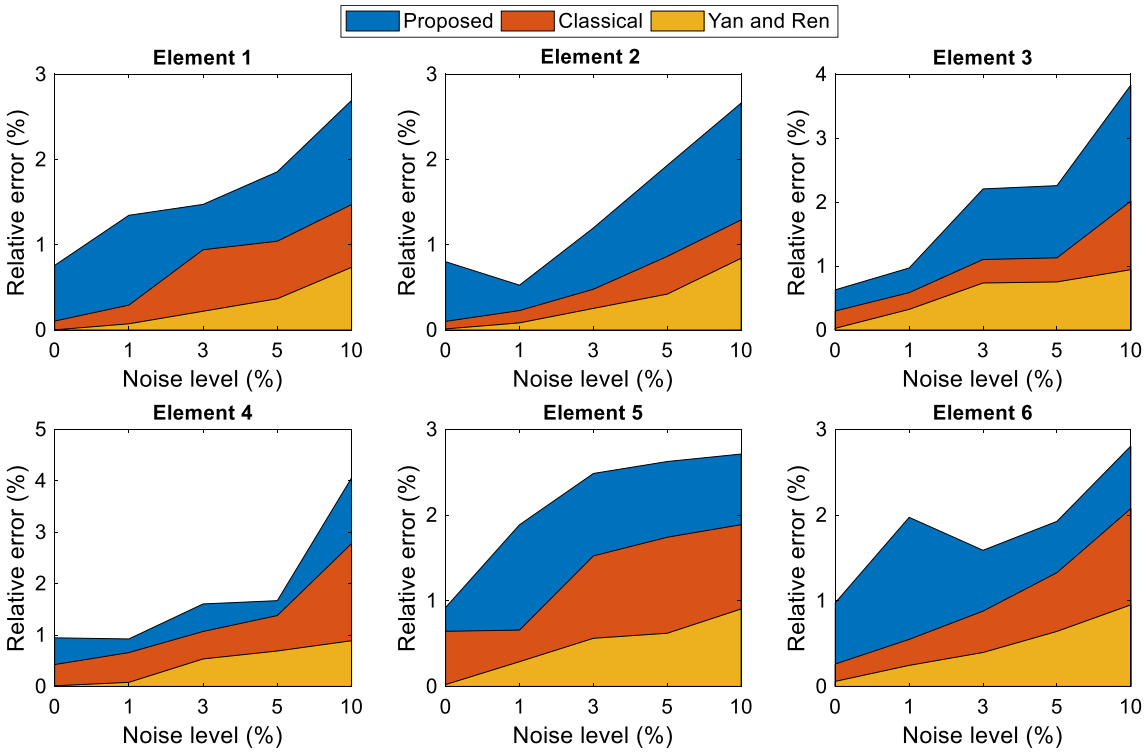

Fig. 6 The comparison of the different sensitivity functions of MSE in Case 2

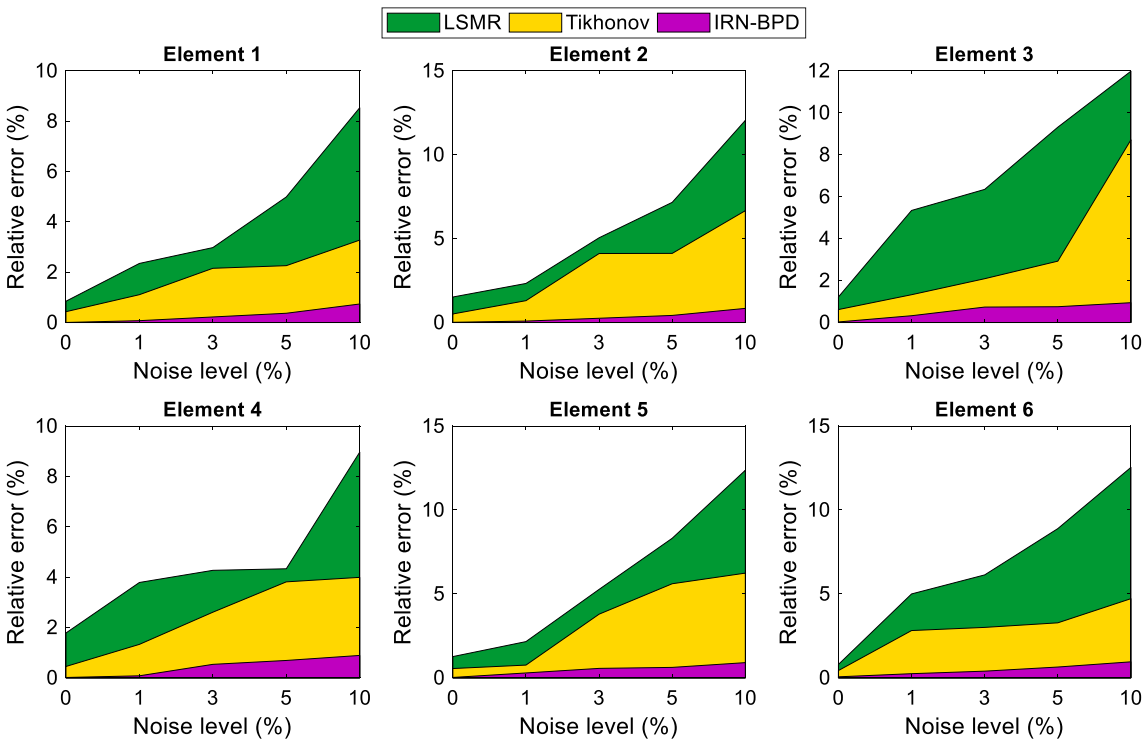

Fig. 7 The comparison of the different regularized solution methods in Case 2

Entezami et al. [8] and Li et al. [22] require determining unknown parameters (i.e., the Lagrange multipliers) and fall in the parametric class of sensitivity formulations, it is neglected to compare the proposed sensitivity function of MSE, which belongs to the non-parametric class, with those functions. For this comparison, the inverse problem of damage identification is solved by the proposed IRN-BPD method. The results of this comparison in Case 2 are shown in Fig. 6. Second, the performance of the proposed IRN-BPD method is evaluated by the Tikhonov regularization (a direct regularized solution) and LSMR (a subspace iterative regularized solution), as illustrated in Fig. 7. Despite reasonable and accurate results of hybrid methods [7, 20], one also neglects to compare IRN-BPD with these approaches due to their complexity. In this comparison, the sensitivity matrix is obtained from the proposed formulation.

As Fig. 6 appears, the best performance in terms of the smallest rate of the relative error is associated with the proposed sensitivity function, particularly in the highest noise level with the errors less than 1%. Although the sensitivity function of Yan and Ren outperforms the classical MSE sensitivity, both of them suffer from larger relative errors than the proposed formulation. Furthermore, one can discern in Fig. 7 that the proposed IRN-BPD method yields smaller relative errors than the Tikhonov regularization and LSMR techniques. This observation indicates the superiority of the proposed regularized solution over the mentioned conventional techniques. From Fig. 7, it is also seen that the direct Tikhonov regularization method performs better than the iterative LSMR technique, in which the number of iterations acts as the regularization value, in terms of the smallest relative error. Therefore, this comparison reveals the positive effect of using a regularization parameter on the solution of the ill-posed inverse problem.

Despite better performance of the proposed IRN-BPD method against the LSMR and Tikhonov regularization techniques in providing more accurate results of the ill-posed inverse problem and damage identification with smaller errors, it is important to compare them in terms of computational efficiency. For this purpose, Table 2 presents the computational time, in the unit of sec, for solving the inverse problem of damage identification in Case 2 under noisy modal data. Note that this comparison is implemented by a laptop featuring an Intel Core i5-5200@2.20 GHz CPU and 8 GB RAM.

Table 2 Computational time (s) for solving the ill-posed inverse problem $\mathbf{Sa} = \mathbf{r}$ regarding the mass–spring system in Case 2 under different noise levels

Noise levels (%)	Methods		
	LSMR	Tikhonov	IRN-BPD
1	6	3	17
3	7	3	18
5	7	2	18
10	7	3	20

As the data in Table 2 appear, the Tikhonov regularization needs shorter time for solving the ill-posed inverse problem in comparison with the iterative solution methods, LSMR and IRN-BPD. In contrast, the proposed method requires longer computational time for solving the problem of interest. It is reasonable, because this method solves the problem in an iterative manner for both obtaining the vector $\mathbf{a}_k$ and the regularization γ_k simultaneously. Regardless of more accurate results of solution obtained from IRN-BPD, it should be noted that although this method needs longer time, the time amounts are not considerable for concluding that it is computationally inefficient.

6.2 The I-40 bridge

For further investigation using a more rigorous numerical model than the previous example, this section aims at validating the proposed methods by a numerical simulation of a full-scale structure. This simulation is implemented on the I-40 bridge, as shown in Fig. 8a, located along Interstate Highway 40 across the Rio Grande River in Albuquerque, New Mexico, USA [33]. The I-40 bridge included twin spans with separate highways for each traffic direction. This structure was constructed from a concrete deck containing a wide of 13.3 m and a thickness of 0.178 m. The deck was supported by two steel plate girders and three steel stringers. Figure 8b depicts the cross-section of the bridge deck. External loads caused by traffics from the stringers were transformed to the steel plate girders by the floor beams. Furthermore, cross-bracing was also provided between the floor beams.

The section that was instrumented with some sensors in its experimental study [34] is applied to construct the numerical or FE model of the I-40 bridge. This section, which is illustrated in Fig. 8c, was composed of three spans with a combined length of 129.5 m, so that the first and third spans had an equal length of 39.9 m, and the length of the middle span was identical to 49.7 m. To avoid challenges related to model updating, the numerical models of the I-40 bridge in the undamaged and damaged states are considered to identify simulated damage cases. Due to use of the numerical models, it is feasible to evaluate more damage patterns compared to the experimental case study [34].

The numerical model of the I-40 bridge is constructed in the MATLAB environment using shell and 3D beam elements [35]. Figure 9 shows the element numbers of the concrete deck, the girder webs, and the piers. The concrete deck and the girder webs are modeled using 144 and 48 four-node shell elements, each of which consists of the membrane and

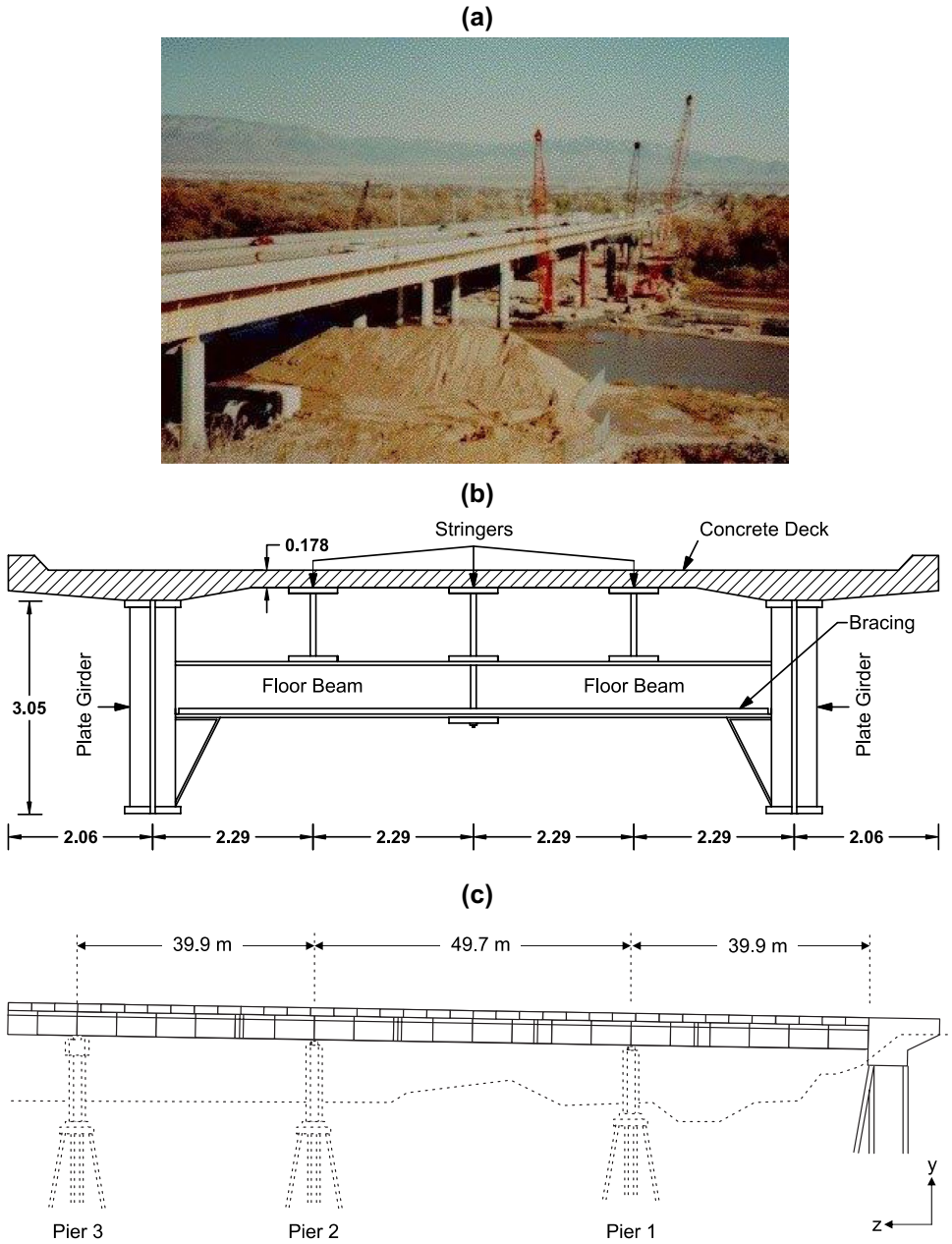

Fig. 8 **a** The image of the I-40 bridge; **b** the cross-section; **c** the elevation view

rectangular plate elements. In Fig. 9a, the elements 1–144 relate to the shell components of the concrete deck. Additionally, the elements 145–168 in Fig. 9b and the elements 169–192 in Fig. 9c are associated with the girder webs on the north and south sides, respectively. The 3D beam elements are utilized to model the top and bottom piers (i.e., the elements 193–204) in Fig. 9b, c and the stringers (W21 × 68) and the floor beams (W36 × 182). Because the stringers and floor beams are not considered to use in the process of damage identification, it is neglected to define their element labels and numbers. Nonetheless, those are incorporated in numerical modeling. The materials used in the I-40 bridge were concrete and steel. Hence, the modulus of elasticity, density, and the Passion's ratio needed for the numerical modeling are identical to 24.8 GPa, 2322.6 kg/m^3, and 0.2 for concrete and 210 GPa, 7850 kg/m^3, and 0.3 for steel, respectively. Moreover, the model of the concrete deck is simplified using a constant thickness of 0.2209 m without considering the steel rebars.

Once the numerical model has been modeled, which refers to the undamaged state of the bridge, simulated damage cases are defined as reductions in stiffness (the flexural rigidity) of some elements to model the damaged conditions as listed in Table 3. To simulate the incompleteness conditions of the modal data, one assumes that the only vertical and horizontal DOFs at the simulated sensors from

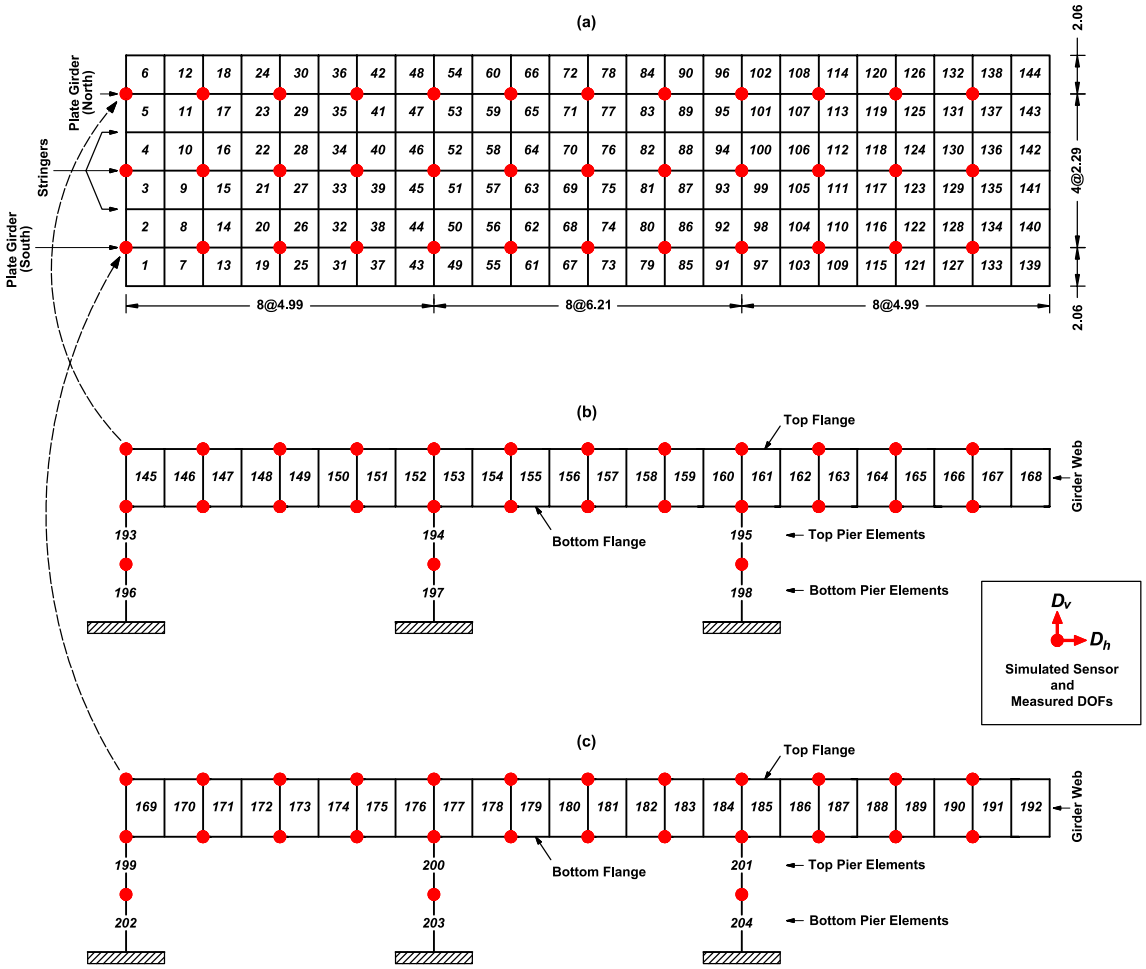

Fig. 9 The numerical model and element numbers of the I-40 bridge: **a** the concrete deck, **b** the north girder and piers, and **c** the south girder and piers (D_h horizontal DOF, D_v vertical DOF)

Table 3 Simulated damage cases for the numerical study of the I-40 bridge

Case no.	Damage locations (elements)	Damage severity (%)
1	63, 64, 69, 70, 75, 76	−20
2	155, 156, 157	−20
3	164, 172, 179	−20, −25, −20
	197, 202	−30, −20
4	17, 62, 93, 112	−20, −40, −30, −20
	155, 189	−30, −20
	196, 204	−20, −30

six modes ($m=6$) are only measurable. Such simulated sensors and measured DOFs are observable in Fig. 9. Applying the mass and stiffness matrices of the FE model of the I-40 bridge, the full sets of the analytical modal parameters can be obtained using the generalized eigenvalue problem. Similar to the previous numerical example, the incomplete mode shapes of the damaged states are initially scaled by the modal scale factor. Next, the SEREP technique is utilized to expand the incomplete mass-normalized modal vectors. Furthermore, the noise levels equal to 3% and 10% are considered to simulate the noisy modal data.

Table 4 The iteration numbers for solving the inverse problem of damage identification by IRN-BPD

Noise levels (%)	Case no.			
	1	2	3	4
3	82	76	76	81
10	127	122	127	133

Having constructed the sensitivity matrix **S** and the residual vector **r**, the inverse problem of damage identification **Sa** = **r** is solved by the proposed IRN-BPD method under the mentioned noise levels. Table 4 presents the number of iterations needed for solving the inverse problem. Additionally, Fig. 10 and Fig. 11 display the convergence rates in all cases

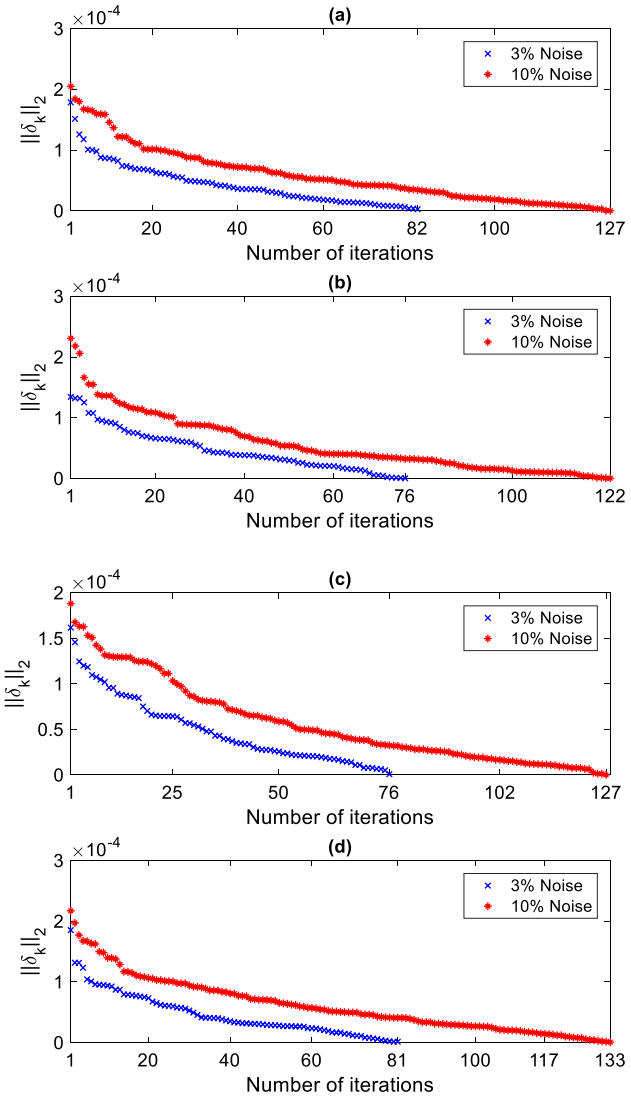

Fig. 10 Convergence rates of the solution of the inverse problem using the l_2-norm of $\boldsymbol{\delta}_k$: **a** Case 1, **b** Case 2, **c** Case 3, and **d** Case 4

and the process of determining the optimal regularization parameters for Case 1, respectively. The stopping condition for terminating the iterative algorithm of IRN-BPD is set as $e = 1\text{e}{-5}$. As can be seen in Fig. 11, the optimal values of γ_k are chosen at the last iterations. Obtaining the solution vector **a** in the two noise levels, Figs. 12, 13, 14, and 15 indicate the results of damage localization and quantification in Cases 1–4, respectively.

From Fig. 12, one can observe that the concrete deck elements 63, 64, 69, 70, 75, and 76 are the damaged areas of the I-40 bridge in Case 1 for both the noise levels. The amounts of |**a**| or the absolute values of the stiffness reduction factor at these locations are identical to 0.1955, 0.1947, 0.1944, 0.1958, 0.1950, and 0.1944 in the 3% noise level and 0.1921, 0.1928, 0.1912, 0.1918, 0.1920, and 0.1904 in the 10% noise level. These amounts disclose that the relative errors in quantifying damage are less than 3% and 5% in the 3% and 10% noise levels, respectively.

Moreover, the maximum errors in the undamaged elements of Case 1 correspond to 2.92% and 3.61% in these levels, respectively. In Fig. 13, it is seen that the elements 155–157 in the north girder are the damaged areas in Case 2. The values of |**a**| at these elements are equal to 0.1967, 0.1971, and 0.1953 in the 3% noise level (i.e., the maximum relative error of 2.35%) and 0.1911, 0.1905, and 0.1899 in the 10% noise level (i.e., the maximum relative error of 5.05%). Moreover, the maximum errors in the undamaged elements in Fig. 13 correspond to 2.09% and 3.79% for the mentioned noise levels. On the other hand, the damage locations as well as the amounts of |**a**| in Cases 3 and 4 are shown in Figs. 14 and 15, respectively. In these figures, the maximum relative errors in the 3% and 10% noise levels are equal to 2.68% and 4.61%, respectively. All the obtained results in Figs. 12, 13, 14, and 15 confirm that the proposed sensitivity function and IRN-BPD succeed in locating and quantifying damage under noisy modal data.

Similar to the preceding example, Fig. 16 shows the comparisons among the proposed, classical, and Yan and Ren's sensitivity functions in locating and quantifying the damage in Case 4 by considering the 3% and 10% noise levels. Moreover, Fig. 17 indicates the comparisons among IRN-BPD, LSMR, and Tikhonov regularization in Case 4 under the two noise levels using the proposed sensitivity of MSE. As

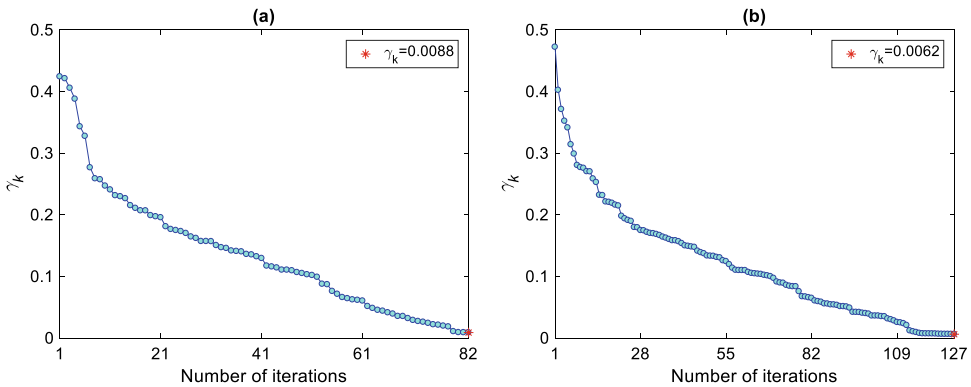

Fig. 11 Determination of the optimal regularization parameters via the improved GCV function in Case 1: **a** 3% noise; **b** 10% noise

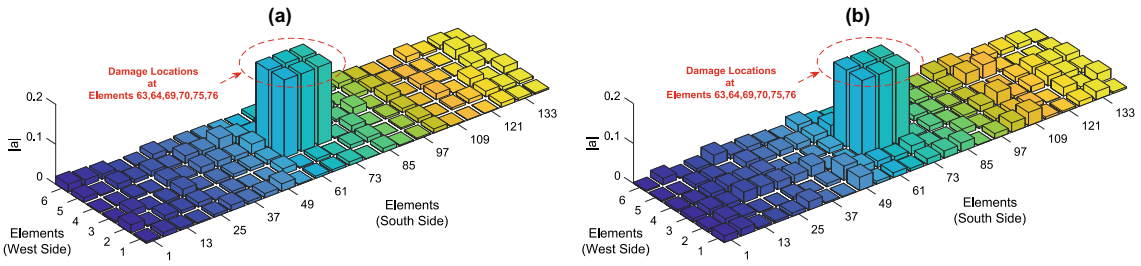

Fig. 12 Damage localization and quantification in Case 1: **a** 3% noise; **b** 10% noise

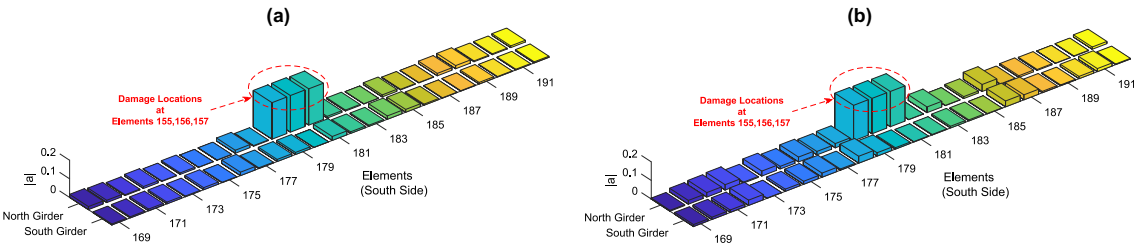

Fig. 13 Damage localization and quantification in Case 2: **a** 3% noise; **b** 10% noise

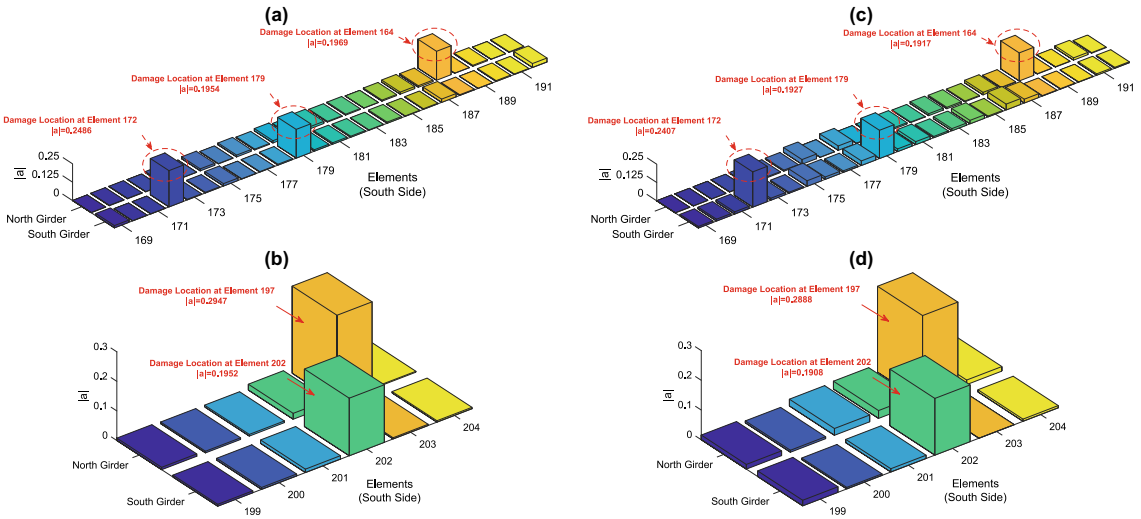

Fig. 14 Damage localization and quantification in Case 3: **a** the girder elements in the 3% noise level, **b** the pier elements in the 3% noise level, **c** the girder elements in the 10% noise level, **d** the pier elements in the 10% noise level

Fig. 16 appears, the relative errors regarding the proposed sensitivity function of MSE are smaller than the corresponding errors associated with the classical formulation as well as Yan and Ren's sensitivity. In addition, one can observe that the sensitivity formulation proposed by Yan and Ren is better than the classical formulation in the aspect of having smaller errors. On the other hand, the amounts of relative errors in Fig. 17 demonstrate that the proposed IRN-BPD method outperforms the LSMR and Tikhonov regularization techniques owing to its smaller errors. It is also observed that the Tikhonov regularization method is more successful in solving the ill-posed inverse problem compared to the LSMR technique. It should be noted that the same conclusions are also valid for other cases. Therefore, the results of comparative analyses prove the superiority of the proposed sensitivity function and IRN-BPD over their counterparts.

On the other hand, the other comparison is to evaluate the computational time for solving the ill-posed inverse problem by IRN-BPD, Tikhonov regularization, and LSMR, as presented in Table 5. For this comparison, all damaged

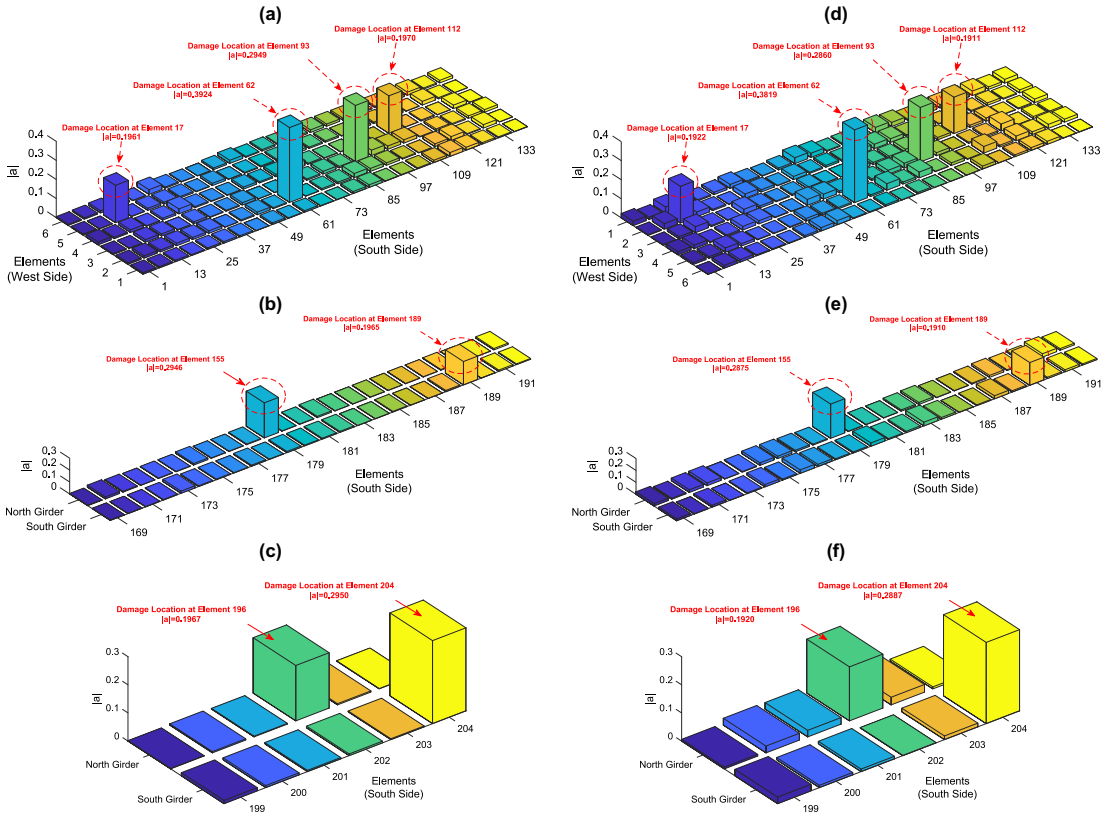

Fig. 15 Damage localization and quantification in Case 4: **a** the deck elements in the 3% noise level, **b** the girder elements in the 3% noise level, **c** the pier elements in the 3% noise level, **d** the deck elements in the 10% noise level, **e** the girder elements in the 10% noise level, and **f** the pier elements in the 10% noise level

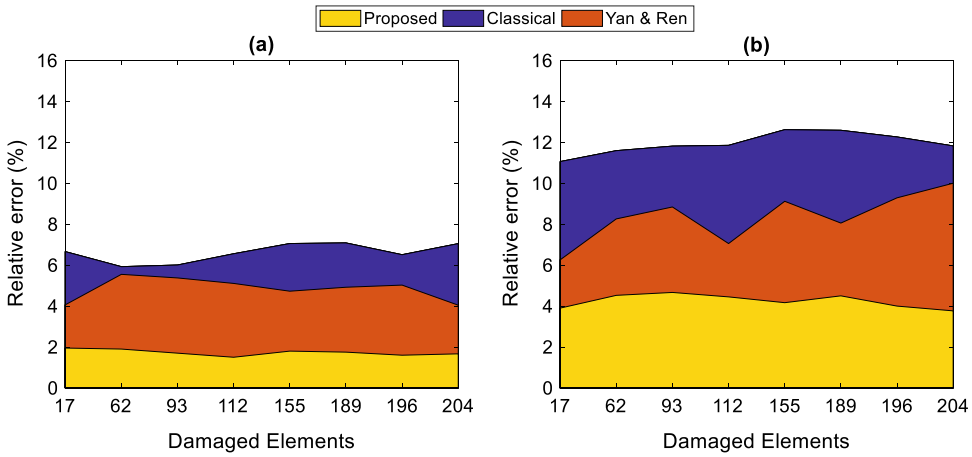

Fig. 16 The comparison of the different MSE sensitivity functions in Case 4: **a** 3% noise; **b** 10% noise

cases and noise levels are considered. As can be observed, the Tikhonov regularization technique needs shorter time for solving the inverse problem, due to its non-iterative nature, compared to the iterative solution approaches. By contrast, the proposed IRN-BPD takes longer time for solving the problem of interest. This is also reasonable, since this method requires solving $\mathbf{Sa} = \mathbf{r}$ in an iterative manner and simultaneously determining the regularization value γ_k. Hence, as the number of iterations increases, the computational time increases as well. However, the time amounts in Table 5 regarding IRN-BPD are not substantial by considering the noise levels, the number of elements, and complexity of the model. Therefore, it is difficult to state that this method is computationally inefficient.

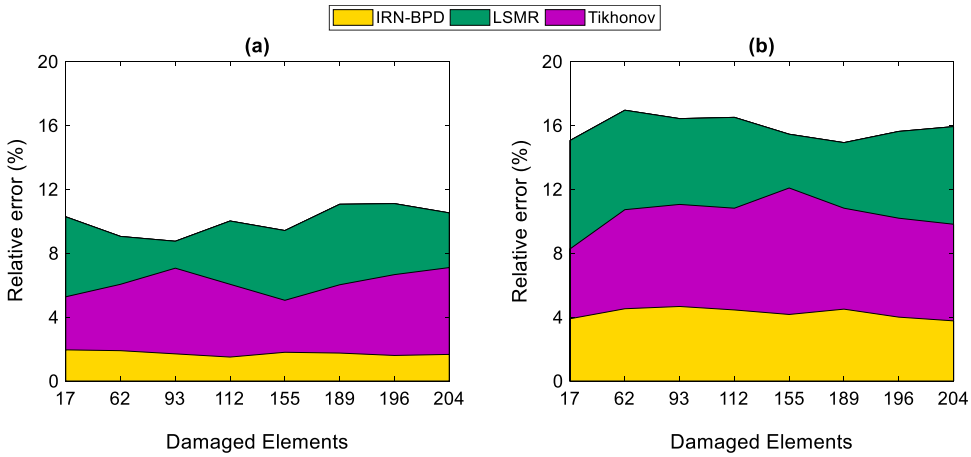

Fig. 17 The comparison of the different regularized solution methods in Case 4: **a** 3% noise; **b** 10% noise

Table 5 Computational time (s) for solving the ill-posed inverse problem $\mathbf{Sa}=\mathbf{r}$ regarding the I-40 Bridge in all cases under different noise levels

Noise levels (%)	Case no.	Methods		
		LSMR	Tikhonov	IRN-BPD
3	1	13	6	33
	2	14	6	25
	3	14	7	25
	4	14	8	25
10	1	15	10	56
	2	19	10	52
	3	19	10	54
	4	21	11	57

In the problem of damage diagnosis based on the concept of model updating, it is considered that the FE model of the structure, which refers to its normal condition, should be as close as the real model. Hence, one attempts to prepare such a numerical model after some model updating procedures [8, 36]. Nevertheless, since any FE model can be a simplified representation of a real structure, modeling errors such as an inaccurate estimation of the mass matrix often exist and may result in a systematic error in detecting, locating, and quantifying damage. Although structural damage does not affect the mass parameters, an inaccurate or unreliable assumption of the mass properties may cause errors in estimating the mode shapes and natural frequencies of the FE model (i.e., analytical or numerical data). Since these modal parameters are utilized to construct the sensitivity matrix, this issue may affect the problem of damage diagnosis [36, 37]. With these descriptions, distributed mass errors including 1%, 5%, and 10% are added to all elements separately and individually to investigate the performance of the proposed method under these modeling errors.

To evaluate the influence of these modeling errors on the performance of the proposed method, the relative errors in quantifying damage concerning Case 4 under 3% and 10% noise levels are incorporated. Figure 18 shows the computed relative errors at the damaged elements of Case 4 in the case of no modeling error (i.e., the condition without the mass errors regarding the previous results) and the three mentioned errors. As can be seen, the amounts of the relative

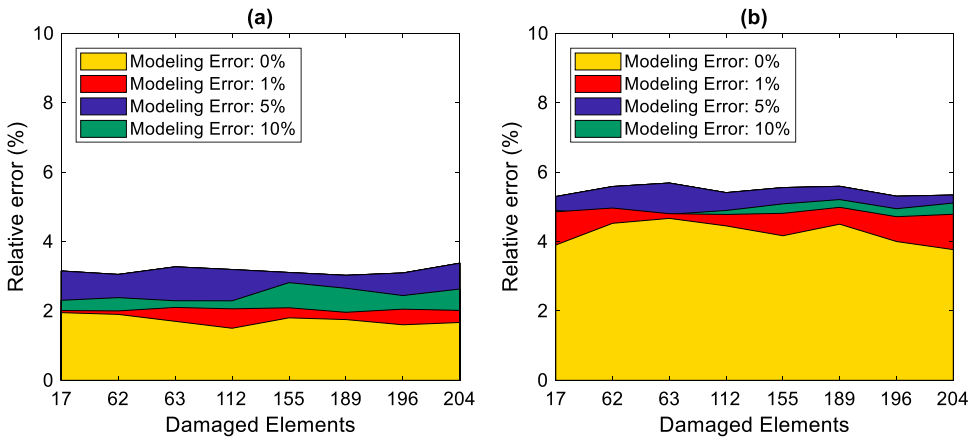

Fig. 18 Performance evaluation of the proposed method under different mass modeling errors in Case 4: **a** 3% noise; **b** 10% noise

errors are roughly in the same range, i.e., smaller than 4% in Fig. 18a and 6% in Fig. 18b. It is important to mention that the maximum relative errors in the undamaged areas of Case 4 for 1, 5, and 10% mass modeling errors correspond to 3.01%, 3.66%, and 3.81% in 3% noise level and 4.62%, 5.18%, and 5.22% in 10% noise level, respectively. All these conclusions demonstrate that the proposed IRN-BPD method in cooperation with the proposed sensitivity function succeeds in locating and quantifying damage even under the mass modeling errors.

The other important issue in model-based strategies pertains to the problem of deploying a limited number of sensors. Since the previous results have been based on a densely sensor networks (i.e., the red nodes on the deck, the bottom flanges of the north and south girders, and the middle of the columns), as shown in Fig. 9, it is necessary to conduct a comparative study for assessing the influence of the number of sensors on the performance of the proposed method. Notice that the nodes on the top flanges of the north and south girders and the nodes on the deck related to these girders are equivalent. For this purpose, three different simulations are considered by decreasing the simulated sensors as presented in Table 6.

In all these cases, it is attempted to choose some nodes (i.e., both the vertical and horizontal DOFs) of the deck, bottom flanges, and columns without knowing the damaged elements of Case 4. In Table 6, the first scenario refers to the initial consideration of the simulated sensors for damage diagnosis. The second scenario uses 50% of the simulated sensors on the deck and bottom flanges of the north and south girders as well as all sensors on the middle of the columns. In the third and fourth deployment scenarios, 25% of the simulated sensors on the decks and bottom flanges without any sensors on the columns are considered. The main difference between these scenarios is to select various (limited) sensors on the deck and bottom flanges. It should be mentioned that the selected sensors of the fourth scenarios are farther from the damaged elements of Case 4 compared with the third scenario.

Table 6 Different scenarios of sensor simulations in the i-40 bridge

Scenario no.	Bridge areas for sensor deployment			Total
	Deck	Bottom flanges	Columns	
1	36	24	6	66
2	18	12	6	36
3	9	6	–	15
4	9	6	–	15

By implementing all steps of the sensitivity-based damage diagnosis, Fig. 19 shows the relative errors at the damaged elements of Case 4 in 3% and 10% noise levels under the defined scenarios of the sensor deployments. From Fig. 19, it can be discerned that the first and second scenarios approximately yield similar performances (i.e., the amounts of the relative errors are smaller than 3% and 6% related to the 3% and 10% noise levels); however, the second scenario slightly has more errors in comparison with the first one. Regarding the third and fourth scenarios, some inconsiderable increases in the relative errors of the damaged elements, with the exception of the elements 196 and 204, are also observable. Regardless of these elements, it is seen that the relative errors are smaller than 5% and 8% in the first and second noise levels, respectively. The main reasons for sudden increases in the relative errors at the elements 196 and 204 are most likely related to the lack of assignment of the simulated sensors on the middle of the columns or the poor performance of the SEREP technique for expanding the mode shapes of the DOFs of these elements. By comparing the error values in Fig. 19, thus, one can conclude that the use of adequate sensors and consideration of an optimal sensor placement are effective for having a reliable damage localization and quantification.

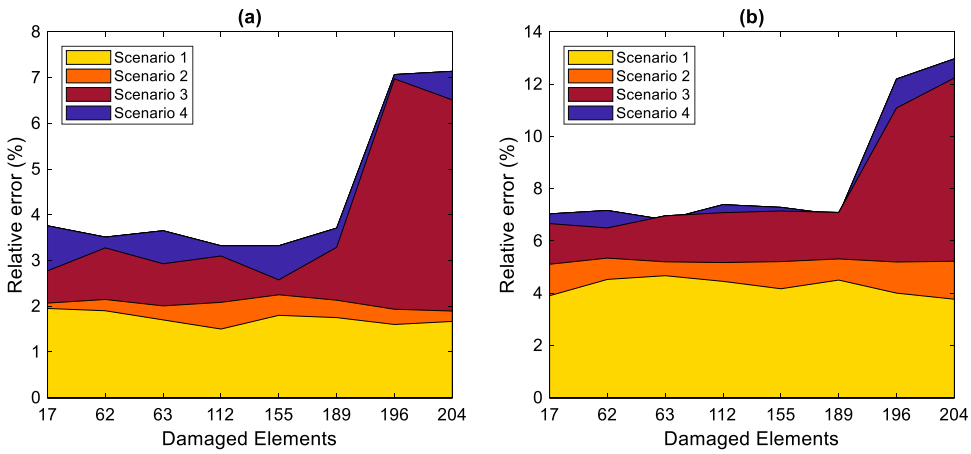

Fig. 19 Performance evaluation of the proposed method under different sensor deployments in Case 4: **a** 3% noise; **b** 10% noise

7 Conclusions

In this study, a new sensitivity-based damage identification method under the model updating strategy has been proposed to locate and quantify structural damage using incomplete noisy modal data. A new sensitivity function of MSE has been developed to improve the classical sensitivity formulation by getting idea from the first-order necessary condition of the optimization problem and adding a term associated with the variation in structural stiffness as the main damage index to the derivatives of eigenvalue and eigenvector. The IRN-BPD method has been presented to solve the inverse problem of damage identification in an iterative manner. A stopping condition and an improved GCV function have also been proposed to terminate the iterative algorithm of IRN-BPD and choose an optimal regularization value. Eventually, the accuracy and performance of the proposed methods have been verified by the mass–spring system and the I-40 bridge in numerical studies.

The results have demonstrated that the proposed sensitivity function of MSE is sensitive to damage and has sufficient damage detectability. It has been observed that the proposed methods succeed in locating and quantifying damage even under the noisy modal data. The comparisons among different sensitivity formulations have revealed that the proposed function outperforms the classical sensitivity functions of MSE. Moreover, the comparative analyses on the performances of different regularized solution approaches have indicated that the proposed IRN-BPD method is superior to the LSMR and Tikhonov regularization techniques in the aspect of having smaller relative errors. Regarding the computational time, it has been seen that the Tikhonov regularization and IRN-BPD had the shortest and longest computational time for solving the ill-posed inverse problem of damage identification, respectively. However, the time amounts regarding the proposed method have not been considerable for concluding that it is computationally inefficient. The performance evaluation of the proposed method and sensitivity function under different mass modeling errors has demonstrated that they are still successful in accurately locating and quantifying damage. By considering different sensor deployments and reducing their numbers regarding the numerical problem of the I-40 bridge, the comparison results have shown that the reductions in the simulated sensors and changes in their deployments do not significantly affect the performance of the proposed method until an important part of the structure (e.g., the bridge columns in this research) has not been equipped with adequate sensors. For this reason, an optimal sensor placement and consideration of adequate and effective sensors are importance to the problem of damage diagnosis.

Despite reasonable and reliable results of damage diagnosis in this research, the proposed sensitivity function and regularized solution have only been verified numerically. Due to the importance of an experimental validation, it is recommended to verify the proposed methods by experimental data of full-scale or laboratory structures.

Declarations

Conflict of interest The authors would like to declare that there is no conflict of interest.

References

1. Yan Y, Cheng L, Wu Z, Yam L (2007) Development in vibration-based structural damage detection technique. Mech Syst Sig Process 21(5):2198–2211
2. Das S, Saha P, Patro S (2016) Vibration-based damage detection techniques used for health monitoring of structures: a review. J Civ Struct Health Monit 6(3):477–507
3. Daneshvar MH, Gharighoran A, Zareei SA, Karamodin A (2021) Early damage detection under massive data via innovative hybrid methods: application to a large-scale cable-stayed bridge. Struct Infrastruct Eng 17(7):902–920. https://doi.org/10.1080/15732479.2020.1777572
4. Sarmadi H, Karamodin A (2020) A novel anomaly detection method based on adaptive Mahalanobis-squared distance and one-class kNN rule for structural health monitoring under environmental effects. Mech Syst Sig Process 140:106495. https://doi.org/10.1016/j.ymssp.2019.106495
5. Sarmadi H, Entezami A, Saeedi Razavi B, Yuen K-V (2021) Ensemble learning-based structural health monitoring by Mahalanobis distance metrics. Struct Contr Health Monit 28(2):e2663. https://doi.org/10.1002/stc.2663
6. Sarmadi H, Yuen K-V (2021) Early damage detection by an innovative unsupervised learning method based on kernel null space and peak-over-threshold. Comput Aided Civ Inf 36(9):1150–1167. https://doi.org/10.1111/mice.12635
7. Sarmadi H, Entezami A, Ghalehnovi M (2020) On model-based damage detection by an enhanced sensitivity function of modal flexibility and LSMR-Tikhonov method under incomplete noisy modal data. Eng Comput. https://doi.org/10.1007/s00366-020-01041-8
8. Entezami A, Shariatmadar H, Sarmadi H (2017) Structural damage detection by a new iterative regularization method and an improved sensitivity function. J Sound Vibrat 399:285–307. https://doi.org/10.1016/j.jsv.2017.02.038
9. Sarmadi H, Entezami A, Daneshvar Khorram M (2020) Energy-based damage localization under ambient vibration and non-stationary signals by ensemble empirical mode decomposition and Mahalanobis-squared distance. J Vibrat Control 26(11–12):1012–1027. https://doi.org/10.1177/1077546319891306
10. Daneshvar MH, Gharighoran A, Zareei SA, Karamodin A (2021) Structural health monitoring using high-dimensional features from time series modeling by innovative hybrid distance-based methods. J Civ Struct Health Monit 11(2):537–557. https://doi.org/10.1007/s13349-020-00466-5
11. Ghasemi MR, Nobahari M, Shabakhty N (2018) Enhanced optimization-based structural damage detection method using modal

strain energy and modal frequencies. Eng Comput 34(3):637–647. https://doi.org/10.1007/s00366-017-0563-5
12. Lee E-T, Eun H-C (2019) Model-based damage detection using constraint forces at measurements. Eng Comput. https://doi.org/10.1007/s00366-019-00762-9
13. Ghiasi R, Fathnejat H, Torkzadeh P (2019) A three-stage damage detection method for large-scale space structures using forward substructuring approach and enhanced bat optimization algorithm. Eng Comput 35(3):857–874. https://doi.org/10.1007/s00366-018-0636-0
14. Gomes GF, Giovani RS (2020) An efficient two-step damage identification method using sunflower optimization algorithm and mode shape curvature (MSDBI–SFO). Eng Comput. https://doi.org/10.1007/s00366-020-01128-2
15. Entezami A, Shariatmadar H, Karamodin A (2019) Data-driven damage diagnosis under environmental and operational variability by novel statistical pattern recognition methods. Struct Health Monit 18(5–6):1416–1443
16. Worden K, Farrar C, Manson G, Park G (2007) The fundamental axioms of structural health monitoring. Proc R Soc A Math Phys Eng Sci 463(2082):1639
17. Rezaiee-Pajand M, Sarmadi H, Entezami A (2021) A hybrid sensitivity function and Lanczos bidiagonalization-Tikhonov method for structural model updating: application to a full-scale bridge structure. Appl Math Model 89:860–884. https://doi.org/10.1016/j.apm.2020.07.044
18. Lin R, Mottershead J, Ng T (2020) A state-of-the-art review on theory and engineering applications of eigenvalue and eigenvector derivatives. Mech Syst Sig Process 138:106536
19. Mottershead JE, Link M, Friswell MI (2011) The sensitivity method in finite element model updating: a tutorial. Mech Syst Sig Process 25(7):2275–2296. https://doi.org/10.1016/j.ymssp.2010.10.012
20. Rezaiee-Pajand M, Entezami A, Sarmadi H (2020) A sensitivity-based finite element model updating based on unconstrained optimization problem and regularized solution methods. Struct Contr Health Monit 27(5):e2481. https://doi.org/10.1002/stc.2481
21. Yan WJ, Ren WX (2011) A direct algebraic method to calculate the sensitivity of element modal strain energy. Int J Numer Method Biomed Eng 27:694–710
22. Li L, Hu Y, Wang X (2013) Numerical methods for evaluating the sensitivity of element modal strain energy. Finite Elem Anal Des 64:13–23. https://doi.org/10.1016/j.finel.2012.09.006
23. Titurus B, Friswell M (2008) Regularization in model updating. Int J Numer Meth Eng 75(4):440–478
24. Sarmadi H, Karamodin A, Entezami A (2016) A new iterative model updating technique based on least squares minimal residual method using measured modal data. Appl Math Model 40(23):10323–10341. https://doi.org/10.1016/j.apm.2016.07.015
25. Kilmer ME, O'Leary DP (2001) Choosing regularization parameters in iterative methods for ill-posed problems. SIAM J Matrix Anal Appl 22(4):1204–1221
26. Rodriguez P, Wohlberg B An efficient algorithm for sparse representations with lp data fidelity term. In: Proceedings of 4th IEEE Andean Technical Conference (ANDESCON), 2008
27. Chung J, Palmer K (2015) A hybrid LSMR algorithm for large-scale Tikhonov regularization. SIAM J Sci Comput 37(5):S562–S580
28. Rao SS (2009) Engineering optimization: theory and practice. Wiley, New Jersey
29. Arora JS (2007) Optimization of structural and mechanical systems. World Scientific, Singapore
30. Esfandiari A, Bakhtiari-Nejad F, Rahai A (2013) Theoretical and experimental structural damage diagnosis method using natural frequencies through an improved sensitivity equation. Int J Mech Sci 70:79–89. https://doi.org/10.1016/j.ijmecsci.2013.02.006
31. Hansen PC (2010) Discrete inverse problems: insight and algorithms. Society for Industrial and Applied Mathematics (SIAM), Philadelphia
32. Hou R, Xia Y, Bao Y, Zhou X (2018) Selection of regularization parameter for l1-regularized damage detection. J Sound Vibrat 423:141–160. https://doi.org/10.1016/j.jsv.2018.02.064
33. Farrar CR, Cornwell PJ, Doebling SW, Prime MB (2000) Structural health monitoring studies of the Alamosa Canyon and I-40 bridges. Los Alamos National Lab., NM (US)
34. Farrar CR, Jauregui DA (1998) Comparative study of damage identification algorithms applied to a bridge: I. Experiment. Smart Mater Struct 7:704–719
35. Rao SS (2011) The finite element method in engineering. Elsevier Science, Amsterdam
36. Chen H-P (2008) Application of regularization methods to damage detection in large scale plane frame structures using incomplete noisy modal data. Eng Struct 30(11):3219–3227
37. Esfandiari A (2017) An innovative sensitivity-based method for structural model updating using incomplete modal data. Struct Contr Health Monit 24(4):e1905. https://doi.org/10.1002/stc.1905